Chemical Engineering Journal 503 (2025) 158126

Contents lists available at ScienceDirect

Chemical Engineering Journal

journal homepage: www.elsevier.com/locate/cej

Efficient activation of sodium percarbonate by hydroxylamine-enhanced zero-valent transition metals for the removal of AZO: performance, free radical generation and mechanism

Qiantong Liang [a], Chengyang Nan [a], Xiangwu Huang [a], Qingjin Lin [a], Zhenyun Liang [a], Yu Huang [a], Peihong Zheng [a], Shoupeng Li [a,c,*], Shuiyu Sun [a,b,*]

[a] Guangzhou Key Laboratory Environmental Catalysis and Pollution Control, Guangdong Key Laboratory of Environmental Catalysis and Health Risk Control, School of Environmental Science and Engineering, Institute of Environmental Health and Pollution Control, Guangdong University of Technology, Guangzhou 510006, China
[b] Guangdong Province Solid Waste Recycling and Heavy Metal Pollution Control Engineering Technology Research Center, Guangdong Polytechnic of Environmental Protection Engineering, Foshan 528216, China
[c] Analysis and Test Center, Guangdong University of Technology, Guangzhou 510006, China

ARTICLE INFO

Keywords:
AZO
Hydroxylamine
Zero-valent metal
Sodium percarbonate
Persistent organic pollutants

ABSTRACT

Azoxystrobin (AZO) fungicides are novel organic pollutants which are stable in water environment. These pollutants can be degraded using low cost zero-valent metals (zero-valent iron (ZVI) and zero-valent copper (ZVC)) to activate sodium percarbonate (SPC), and the introduction of hydroxylamine (HA) can effectively improve the reaction efficiency of this system. According to the experimental results, HA significantly promoted the regeneration of Fe^{2+} and Cu^{+} in the decomposed solution of SPC, significantly accelerating the formation of hydroxyl radicals ($^{\bullet}OH$) and facilitating the degradation of AZO. Under optimal conditions, when pH = 3, the rate of AZO removal by the HA/ZVI/SPC system reached 99.0 % in 15 min, while the HA/ZVC/SPC system required 50 min to reach 99.1 % removal. Both of the tested HA/zero-valent metal/SPC processes produced $^{\bullet}OH$, carbonate radicals ($CO_3^{\bullet-}$), superoxide radicals ($O_2^{\bullet-}$) and singlet oxygen ($^1O_2$), among which, $^{\bullet}OH$ appeared to be the main reactant responsible for AZO removal. Furthermore, it was found that $^{\bullet}OH$ reacted with trace levels of carbonate ions to generate other reactive oxygen species and promote AZO degradation. The addition of HA not only slowed down the surface passivation of zero-valent metals, but also promoted the conversion of high-valent metal ions to low-valent metal ions, resulting in the generation of more reactive oxygen species within the system. In addition, the degradation intermediates were identified by LC-MS analysis and density-functional theory (DFT), allowing the possible AZO degradation pathways to be proposed.

1. Introduction

Due to the persistence and toxicity of pesticides, their widespread use presents a serious risk to both environmental and human health [1]. Azoxystrobin (AZO) is an emerging organic pollutant (EOP), which is commonly applied to various crops as a broad-spectrum fungicide. The high stability of AZO and its resistance to natural degradation processes have resulted in its frequent detection in aquatic environments, which may pose a hazard to aquatic organisms [2,3]. For example, in the United States, AZO was the most frequently detected biocide in 103 samples from 29 rivers, with an average concentration of 0.16 μg/L [4,5]. At present, the research on AZO has mainly focused on toxicity analysis, with few studies reporting how to effectively degrade AZO.

Advanced oxidation process can degrade refractory organic pollutants by generating reactive oxygen species. In recent years, sodium percarbonate (SPC, $Na_2CO_3{\cdot}1.5H_2O_2$) has drawn considerable interest as a solid carrier of H_2O_2 (Eq. (1)), providing various benefits including non-toxicity, low environmental impact, long-term storage stability and low explosion risk compared to liquid H_2O_2 [6]. In addition, when SPC is employed as oxidant in advanced oxidation process, its alkaline characteristics ensure wider pH range applicability and prevent unnecessary acidification of water environment [7,8].

$$Na_2CO_3{\cdot}1.5H_2O_2 \rightarrow Na_2CO_3 + 1.5H_2O_2 \quad (1)$$

* Corresponding authors.
E-mail addresses: lsp@gdut.edu.cn (S. Li), sysun@gdut.edu.cn (S. Sun).

https://doi.org/10.1016/j.cej.2024.158126
Received 22 August 2024; Received in revised form 2 November 2024; Accepted 27 November 2024
Available online 30 November 2024

The use of zero-valent metal (ZVM) to activate percarbonates has been shown to be a highly promising strategy for various advanced oxidation process. Among the commonly used ZVMs, zero-valent iron (ZVI) and zero-valent copper (ZVC) are simple to synthesize, widely available, with low environmental impacts and the potential to be applied as substitutes for Fe^{2+} and Cu^{+} due to the continuous release of Fe^{2+} and Cu^{+} through corrosion reactions [9,10].

However, Fe^{3+} and Cu^{2+} generated by the oxidant reactions of ZVI and ZVC, respectively, cannot activate SPC in a sustained and effective manner, reducing the sustainability of the reaction system [11]. The introduction of hydroxylamine (HA) can promote the continuous occurrence of Fenton reaction, rapidly degrade the organic pollutants, and greatly improve the degradation rate of pollutants [12]. In a M_xO_y/PMS system, HA was utilized to speed up the production of Fe^{2+}, Cu^{+}, and Co^{2+} and the removal rate of sulfamethoxazole was increased by 90 % within 30 min [13]. HA also broadens the working pH range. In a neutral environment, the degradation efficiency of orange G was enhanced when HA was added to Fe(II)/PDS [14]. In addition, HA is an essential growth factor for microorganisms, while also achieving a better degradation performance than other reducing agents (such as ascorbic acid) [15]. Earlier studies have mainly concentrated on the enhancing effect of reducing agents on homogeneous Fenton systems. However, the mechanism through which HA promotes AZO degradation by ZVM-activated SPC remains unknown to date. As a result, it is critical to investigate how HA increases AZO degradation and identify the AZO degradation pathways and reaction mechanisms in the two HA/ZVM/SPC systems.

In the present study, AZO was removed in the presence of HA using ZVM (ZVI and ZVC) as SPC activators. The objectives of this study were to: (a) systematically explore the catalytic performance and reaction kinetics of two HA/ZVM/SPC systems under different conditions by choosing AZO as a model contaminant; (b) reveal the reactive oxygen species involved in AZO degradation and the underlying mechanisms of the two HA/ZVM/SPC systems; (c) evaluate the application potential of the two HA/ZVM/SPC systems; (d) explore the AZO degradation pathway by density-functional theory (DFT) calculations and LC-MS analysis, and evaluate the change in toxicity of AZO and its degradation intermediates using the Toxicity Estimation Software Tool (T.E.S.T., v.5.1) and seed germination experiment.

2. Materials and methods

2.1. Chemical materials

The reagents were all above analytical purity, and highly pure reagents were used when testing the metal content. All solutions were prepared from ultra-pure water (resistivity 18.2 MΩ cm^{-1}). Detailed information is provided for all chemicals in the supplementary information (SI) Text S1.

2.2. Experimental process

The degradation test was carried out in a 500 mL beaker. First, the required concentration of AZO standard stock solution (10 mg/L, 200 mL) was added into the beaker. It is worth noting that when SPC is introduced into the system, the pH value of the reaction solution will rise rapidly first, and then remain relatively stable due to its alkaline and buffering properties (Fig. S4). Therefore, before adding specific doses of SPC, HA and ZVM, 1.0 M HCl or NaOH was used to adjust the pH of the initial solution, in order to avoid excessive acidification and effectively inhibit excessive metal ion leaching. Thereafter, the beaker was mechanically agitated at 300 rpm while the water bath temperature was maintained at 25 °C. During this process, 1 mL samples were obtained at different times, and filtered into a brown liquid chromatographic bottle through a 0.22 μm filter. The concentration of AZO was measured by HPLC at 235 nm after the reaction was quenched by the addition of excess methanol (MeOH) [16]. To assess the reusability of ZVM, used ZVI and ZVC were collected by filtration, and then rinsed with ethanol and ultrapure water for three times, and dried under vacuum at 40 °C for subsequent use. In order to differentiate between the active radicals involved, furfuryl alcohol, *tert*-butanol, benzoquinone and phenol were added as scavengers for the quenching experiments [17,18]. Every experiment was run in triplicate.

2.3. Catalyst characterization

A detailed description of the methods used for characterization of ZVI and ZVC particles is given in the SI, Fig. S1 and Text S2.

2.4. Methods of analysis

The concentration of AZO was monitored by high-performance liquid chromatography (HPLC, Agilent 1260 Infinity, USA) equipped with ultraviolet detector at 235 nm wavelength. A C18 column (4 μm, 4.6 × 150 mm) was used for the separation, the mobile phase was made up of acetonitrile and water (v/v = 65:35) at a flow rate of 1 mL·min^{-1} and the injection volume was 10 μL. The operating conditions for sulfonamides (SMX) and ibuprofen (IBU) were: mobile phase of methanol/water (60/40), and detector wavelengths of 256 nm and 220 nm, respectively. The operating conditions for tetracycline (TC) were: mobile phase of 0.01 M oxalic acid/acetonitrile (80/20), and detector wavelength of 360 nm. The operating conditions for ciprofloxacin (CiFX) were: mobile phase of 0.1 % acetic acid/acetonitrile (80/20) and detector wavelength of 278 nm. For thiacloprid (TCP), the operating conditions were: mobile phase of methanol/water (45/55) with detector wavelength of 238 nm [19]. Total organic carbon (TOC) of the reaction solution was detected by TOC analyzer (TOC-VCPH, Shimadzu, Japan). A pH meter (PHS-3C) was used to determine the pH value of the test solution.

The morphology, functional groups, crystal structure and surface electrons of ZVM before use, after reaction without HA and after reaction with HA were analyzed by scanning electron microscope combined with X-ray dispersion spectrometer (SEM-EDS, Sigma 300, Zeiss, Germany), powder X-ray diffraction analyzer (XRD, Ultima IV, Rigaku, Japan) and X-ray photoelectron spectrometer (XPS, K-Alpha, Thermo Scientific, USA).

Concentrations of metal ions, such as iron and copper, were measured using a UV–vis spectrophotometer. Total Fe and Fe^{2+} concentrations were detected by means of a 1,10-phenantroline spectrophotometric method at λ = 510 nm with and without the addition of ascorbic acid. Cu^{2+} and dissolved Cu^{+} were determined using the bis (cyclohexanone) oxaldihydrazone spectrophotometric method at λ = 600 nm, and by 2,9-dimethyl-1,10-phenanthroline method at λ = 457 nm, respectively [20,21]. Total nitrogen (TN) and nitrite nitrogen were analyzed according to the standard method [22]. According to the consensus method, the developmental toxicity and bioaccumulation factors of AZO and its degradation intermediates were evaluated by quantitative structure–activity relationship (QSAR) using the Toxicity Estimation Software Tool (T.E.S.T., v.5.1). High performance liquid chromatography mass spectrometry (LC-MS, 1290/6470, Triple Quad MS, Agilent, USA) was used to analyze the AZO transformation intermediates formed during degradation.

The free radicals $^{\bullet}OH$, the non-radical $^{1}O_2$ and $O_2^{\bullet-}$ in the reaction system were trapped using 2,2,6,6-tetramethyl-4-piperidinol (TEMP) and 5,5-dimethyl-1-pyrroline (DMPO) as trapping agents. Subsequently, the samples were subjected to electron paramagnetic resonance (EPR) analysis to obtain the spectra of $^{\bullet}OH$, $CO_3^{\bullet-}$, $O_2^{\bullet-}$ and $^{1}O_2$. Additionally, the benzoic acid (BA) probe test was used to quantify the concentration of $^{\bullet}OH$ generated inside the reaction system. Eq. (2) was used to compute the $^{\bullet}OH$ concentration [23].

$$Cumulative\left[^{\bullet}OH\right]produced = \left[p - HBA\right] \times 5.87 \quad (2)$$

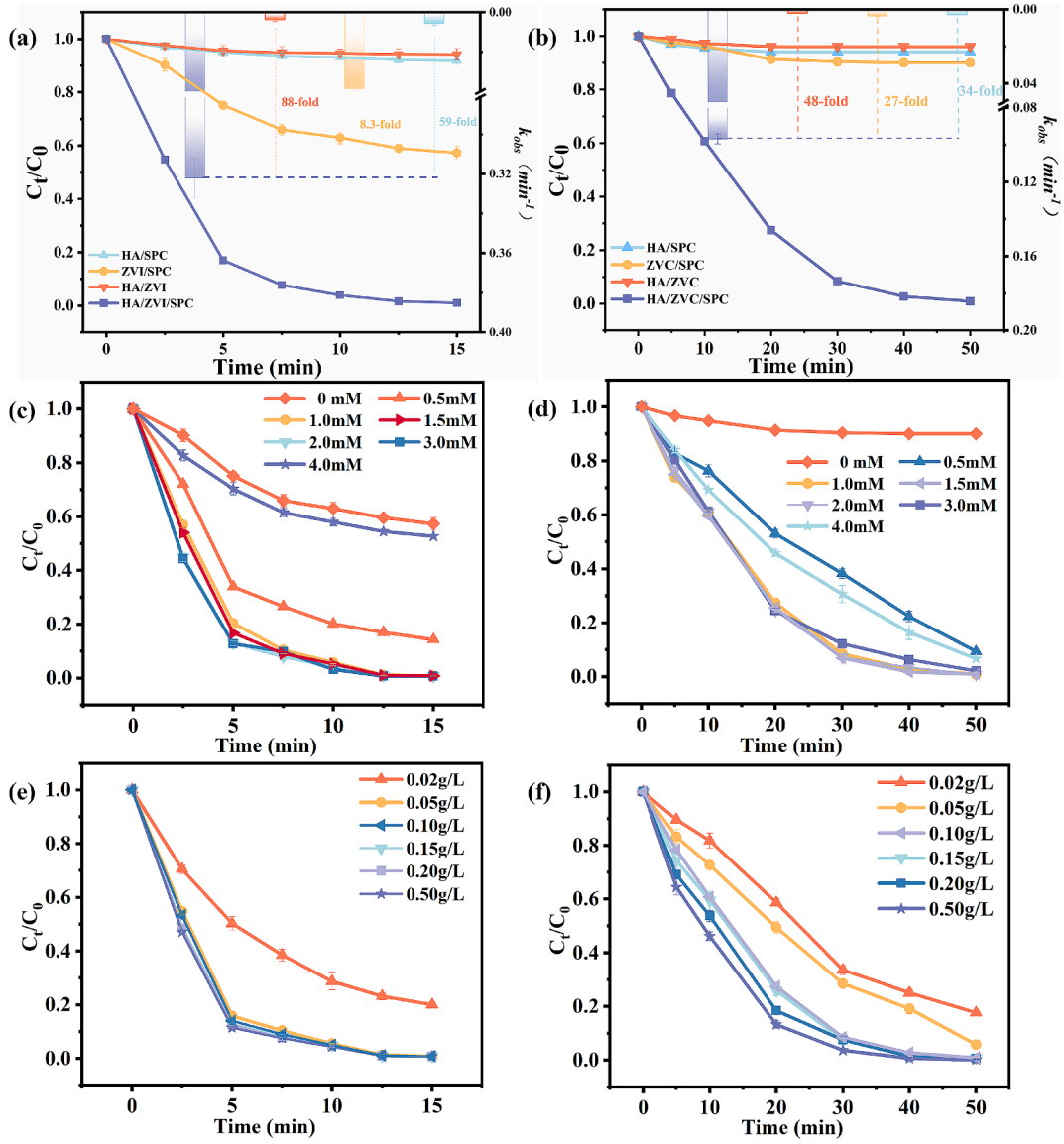

Fig. 1. Removal of AZO by different processes in the (a) ZVI and (b) ZVC systems, reaction conditions:$[ZVI]_0 = 0.05$ g/L, $[ZVC]_0 = 0.10$ g/L, $[SPC]_0 = 1$ mM, $[AZO]_0 = 10$ mg/L, $[HA]_0 = 1$ mM and $[pH]_0 = 3$; Effect of different HA concentrations on the (c) HA/ZVI/SPC and (d) HA/ZVC/SPC systems, reaction conditions:$[ZVI]_0 = 0.05$ g/L, $[ZVC]_0 = 0.10$ g/L, $[SPC]_0 = 1$ mM, $[AZO]_0 = 10$ mg/L, $[HA]_0 = 0$–4 mM and $[pH]_0 = 3$; Effect of different catalyst dosages on the (e) HA/ZVI/SPC and (f) HA/ZVC/SPC systems, reaction conditions:$[ZVI]_0 = 0.02$–0.50 g/L, $[ZVC]_0 = 0.02$–0.50 g/L, $[SPC]_0 = 1$ mM, $[AZO]_0 = 10$ mg/L, $[HA]_0 = 1$ mM and $[pH]_0 = 3$.

In all experiments, AZO degradation followed quasi-primary kinetics, calculated according to the formula shown in Eq. (3).

$$Ln\left(\frac{AZO_t}{AZO_0}\right) = -kobs \cdot t \tag{3}$$

where, AZO_t is the concentration of AZO at a specific reaction time (mg/L); AZO_0 is the initial concentration of AZO (mg/L); k_{obs} represents the first-order rate constant (min^{-1}); and t is the reaction time (min).

2.5. Theoretical calculation and software simulation

Visual MINTEQ software (version 3.1) was employed to model the chemical equilibrium of ions in the water column. The temperature was maintained at 25 ℃, and other parameters were configured based on the actual experimental values.

Gaussian v.09 software was used for all computations. The AZO model was optimized at the 6-31G* basis set level using the B3LYP approach inside the density functional theory (DFT) framework. Frequency calculations and analysis were then performed based on the optimized structures. Gauss View v.6 software was used to view the data [24].

3. Results and discussion

3.1. AZO degradation efficiency of different processes

AZO was degraded by different processes. The degradation of AZO in HA/SPC, ZVM/SPC, HA/ZVM and HA/ZVM.SPC systems at pH = 3 is shown in Fig. 1a and b. Findings indicated that HA/SPC, HA/ZVI and HA/ZVC were unable to effectively degrade AZO, which might be explained by the absence of oxidizing species. About 10 % of AZO was degraded within 50 min in the ZVC/SPC process. In contrast, the combination of ZVI and SPC improved AZO degradation, resulting in 42 % of AZO being degraded within 15 min in the ZVI/SPC process, which may be due to the higher activity of ZVI compared to ZVC. Surprisingly, HA significantly increased the degradation efficiency of the system, with about 99.0 % of AZO degraded within 15 min in the HA/ZVI/SPC

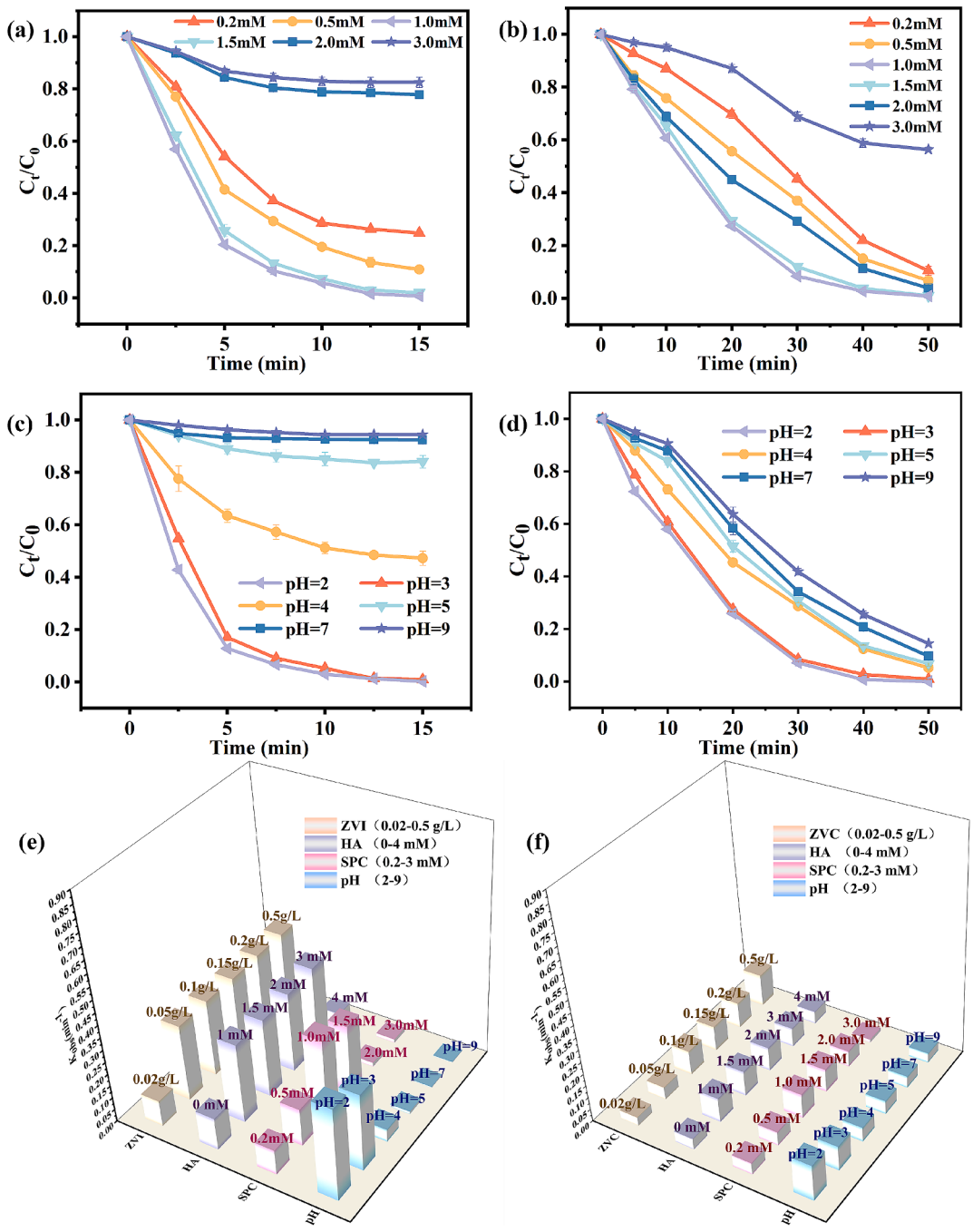

Fig. 2. Effect of different SPC concentrations on the (a) HA/ZVI/SPC and (b) HA/ZVC/SPC systems, reaction conditions:$[ZVI]_0$ = 0.05 g/L, $[ZVC]_0$ = 0.10 g/L, $[SPC]_0$ = 0–3 mM, $[AZO]_0$ = 10 mg/L, $[HA]_0$ = 1 mM and $[pH]_0$ = 3; Effect of initial pH on the (c) HA/ZVI/SPC and (d) HA/ZVC/SPC systems, reaction conditions: $[ZVI]_0$ = 0.05 g/L, $[ZVC]_0$ = 0.10 g/L, $[SPC]_0$ = 1 mM, $[AZO]_0$ = 10 mg/L, $[HA]_0$ = 1 mM and $[pH]_0$ = 2–9; Relationship between k_{obs} values and different key parameters in the (e) HA/ZVI/SPC and (f) HA/ZVC/SPC systems.

system, while in the HA/ZVC/SPC process, 99.1 % AZO degradation required 50 min of reaction time. Therefore, HA plays a significant part in accelerating the removal of AZO in both HA/ZVM/SPC systems. The SPC activation capability of different metal ions is known to vary. The order of sulfamethoxazole degradation by different transition metal activated oxidants, was found to be: Cu(II) < Fe(III) < Cu(I) < Fe(II) [13]. Therefore, it was hypothesized that the addition of HA promoted the increase in Cu^+ and Fe^{2+} concentrations in this experiment. The AZO removal performance of the HA/ZVI/SPC system was higher than that of the HA/ZVC/SPC system due to the higher reduction potential of Fe^{2+} than Cu^+.

In addition, the performance enhancement capability of other reducing agents on the ZVM/SPC system was also compared, including ascorbic acid (AA), citric acid (CA), gallic acid (GA) and anhydrous sulfite (AS) (SI, Fig. S2). Results showed that HA achieved the highest performance enhancement capability compared to the other reducing agents. Ascorbic acid, citric acid, gallic acid and anhydrous sulfite achieved only 65.9 %, 13.4 %, 29.2 % and 10.75 % AZO removal when used for ZVI/SPC system, respectively. This result shows that HA exhibited the highest capability to rapidly reduce Fe^{3+}, while also being less reactive with SPC and the generated reactive oxygen species [25].

3.2. Impact of key parameters on AZO degradation

3.2.1. Impact of HA concentration

Due to the strong reducing properties of HA, it can increase the overall reaction efficiency of the process by promoting the cyclic conversion of high-valent metal ions to low-valent metal ions. In this section, the impact of varying HA concentrations (0, 0.5, 1.0, 1.5, 2.0, 3.0, and 4.0 mM) on the rate of AZO removal was investigated. First, the impact of HA concentration on the breakdown of AZO was examined (Fig. 1c, d). In both HA/ZVM/SPC systems, HA effectively promoted the activation of SPC by ZVM, improving the rate of AZO removal. With the increase in HA concentration, the AZO degradation efficiency of both systems exhibited a trend of initially increasing and then decreasing. For example, in the HA/ZVI/SPC system the AZO degradation efficiency increased from 42.7 % to 99.0 % when the concentration of HA increased from 0 to 3 mM, while the rate of AZO removal decreased to 44.3 % when the concentration of HA increased from 3 to 4 mM. During AZO removal by the ZVM/SPC process, Cu^{2+} and Fe^{3+} were generated due to activation. Under the action of HA, the formed Cu^{2+} and Fe^{3+} ions were reduced to Cu^{+} and Fe^{2+}, leading to the generation of more free radicals and improving the rate of AZO removal. However, excess HA may form excess Cu^{+} and Fe^{2+}, thus competing with the pollutants for free radicals, with excess HA capturing $^{\bullet}OH$ faster and exerting a quenching effect, as described in Eq. (4). Since the removal rate of AZO remained almost unchanged (removal rate $>$ 99 %) when the HA concentration increased from 1 mM to 3 mM in the two HA/ZVM/SPC systems, the HA concentration was set at 1 mM to avoid waste of reagents.

$$NH_2OH + {}^{\bullet}OH \rightarrow OH^{-} + nitrogenousproducts \quad (4)$$

3.2.2. Impact of ZVM concentration on AZO degradation

The increase in ZVM concentration effectively promoted the activation of SPC, enhancing AZO degradation in the two HA/ZVM/SPC systems. In this section, the effects of varying ZVM concentrations (0.02, 0.05, 0.10, 0.15, 0.20, 0.50 g/L) on the rate of AZO removal were investigated. As shown in Fig. 1e and f, with increasing ZVI and ZVC concentrations, the rate of AZO removal in both systems exhibited a continually increasing trend. Taking the HA/ZVI/SPC system as an example, the AZO removal rate increased from 80.3 % to 99.0 % when the concentration of ZVI increased from 0.02 g/L to 0.05 g/L. During oxidant activation by ZVI and ZVC, both metal ions interacted with HA to form Fe^{3+}-HA and Cu^{2+}-HA surface complexes, with HA reducing Fe^{3+} and Cu^{2+} to Fe^{2+} and Cu^{+}. Subsequently, SPC was excited by the released Fe^{2+} and Cu^{+}, generating reactive oxygen species to degrade organic pollutants [26–29]. Therefore, higher ZVI and ZVC concentrations favor AZO degradation. However, when the concentration of ZVI was further increased from 0.05 g/L to 0.5 g/L, the removal rate of AZO hardly changed. This indicates that once sufficient amount of metal ions are available to provide catalytic active sites for SPC activation, further increase in metal ions cannot stimulate additional reactive oxygen species, with the excessive addition of ZVI leading to the reduction of reactive oxygen species and potentially raising the danger of metal ion leaching [30]. Therefore, the optimal metal ion concentrations in the HA/ZVI/SPC and HA/ZVC/SPC systems were 0.05 g/L and 0.10 g/L, respectively.

3.2.3. Impact of SPC concentration on AZO degradation

SPC is the source of reactive oxygen species and plays a crucial role in the degradation of AZO. Hence, the effect of varying SPC concentrations (0.2, 0.5, 1.0, 1.5, 2.0, 3.0 mM) on the rate of AZO removal was investigated. As shown in Fig. 2a and b, in the two HA/ZVM/SPC systems, higher SPC concentration (0.2–1.0 mM) effectively increased the reactive oxygen species yield in the system and enhanced AZO degradation. For instance, in the HA/ZVI/SPC system, the AZO removal rate increased from 75.1 % to 99.0 % after 15 min as the initial SPC concentration increased from 0.2 mM to 1 mM. This may be caused by more reactive oxygen species being produced, which would enhance the degradation of AZO at higher SPC concentration. However, further increasing the SPC concentration to 2 mM (in the two HA/ZVM/SPC systems) resulted in a decrease in the rate of AZO degradation within the same time period, as excess SPC caused the pH of the solution to increase and produced more H_2O_2, triggering free radical quenching as described in Eqs. (5) and (6). Based on the above, the SPC concentration of 1 mM was selected as the ideal dose for the remaining experiments.

$$H_2O_2 + {}^{\bullet}OH \rightarrow H_2O + {}^{\bullet}OOH \quad (5)$$

$$^{\bullet}OOH + {}^{\bullet}OH \rightarrow H_2O + O_2 \quad (6)$$

3.2.4. Impact of initial pH on AZO degradation

The initial pH of the solution has a significant impact on the performance of non-homogeneous advanced oxidation process [30]. The impact of various pH conditions (2, 3, 4, 5, 7, 9) on AZO removal was investigated. As seen from Fig. 2c and d, the impact of pH on AZO degradation varied significantly in the two HA/ZVM/SPC systems. In both HA/ZVM/SPC systems, the highest AZO degradation efficiency was achieved at pH $\leq$ 3. This was particularly true for the HA/ZVI/SPC system, with a significant increase in the AZO removal rate (from 5.6 % to 99.0 %) observed when the pH was decreased from 9 to 3. The system favors the production of reactive oxygen species under acidic conditions, thereby enhancing the degradation of organic matter [30]. When the pH was neutral or alkaline, the rate of reactive oxygen species generation decreased significantly, leading to a notable decline in the rate of organic matter removal [31]. Furthermore, the distribution of iron speciation in solution is influenced by pH value. Visual MINTEQ was used to analyze the distribution of iron speciation (Fig. S3, SI) in the range of pH value from 1.0 to 10.0. The results showed that when the pH value of solution is greater than 3, iron ions gradually decrease, and their precipitation is inevitable. SPC increases the alkalinity of the reaction medium, resulting in a buffering effect, which makes ZVI system particularly sensitive to pH [32].

However, in the HA/ZVC/SPC system, the effect of pH was not as obvious as in the HA/ZVI/SPC system, with the HA/ZVC/SPC process able to degrade pollutants within a wide pH range. At pH = 3, the AZO removal rate in the HA/ZVC/SPC system reached 99.1 % after 50 min and the rate of AZO removal reached more than 90 % when the pH was increased from 4 to 7. However, the rate of AZO removal slightly decreased to 85.5 % at pH = 9 after the solution became alkaline. This was due to the alkaline environment inhibiting the dissolution of Cu ions and the gradual transformation of Cu^{2+} into ions such as $Cu(OH)^{+}$, $Cu(OH)_2$ and $Cu(OH)_3^{-}$, leading to a slowing down of the reaction under alkaline system pH conditions [33]. In addition, the oxidation potential of $^{\bullet}OH$ decreased in high pH environments. Due to its unstable nature, H_2O_2 was self-decomposed into H_2O and O_2, which was unfavorable for subsequent conversion into other reactive oxygen species [34]. Furthermore, the presence of alkaline conditions resulted in a higher level of metal ion precipitation, which was unfavorable for the ongoing generation of Fe^{2+} and Cu^{+} and thereby reduced the availability of catalytic sites on the surface of ZVM [35]. Although the optimal reaction pH for both HA/ZVM/SPC systems was pH = 2, adjusting the system to a pH = 2 solution in practical applications consumes a large amount of acid and causes corrosion to the instruments and pipelines. Therefore, in this study, system performances were explored at pH = 3 [36].

3.3. Role of inorganic ions and NOM

The degradation of target pollutants may be impacted by the presence of natural organic matter (NOM) and inorganic anions in natural waters. Therefore, it is necessary to establish whether common anions such as 20 mM HCO_3^{-}, Cl^{-}, SO_4^{2-}, NO_2^{-} and 50 mg/L humic acid can affect pollutant removal during the practical application of advanced

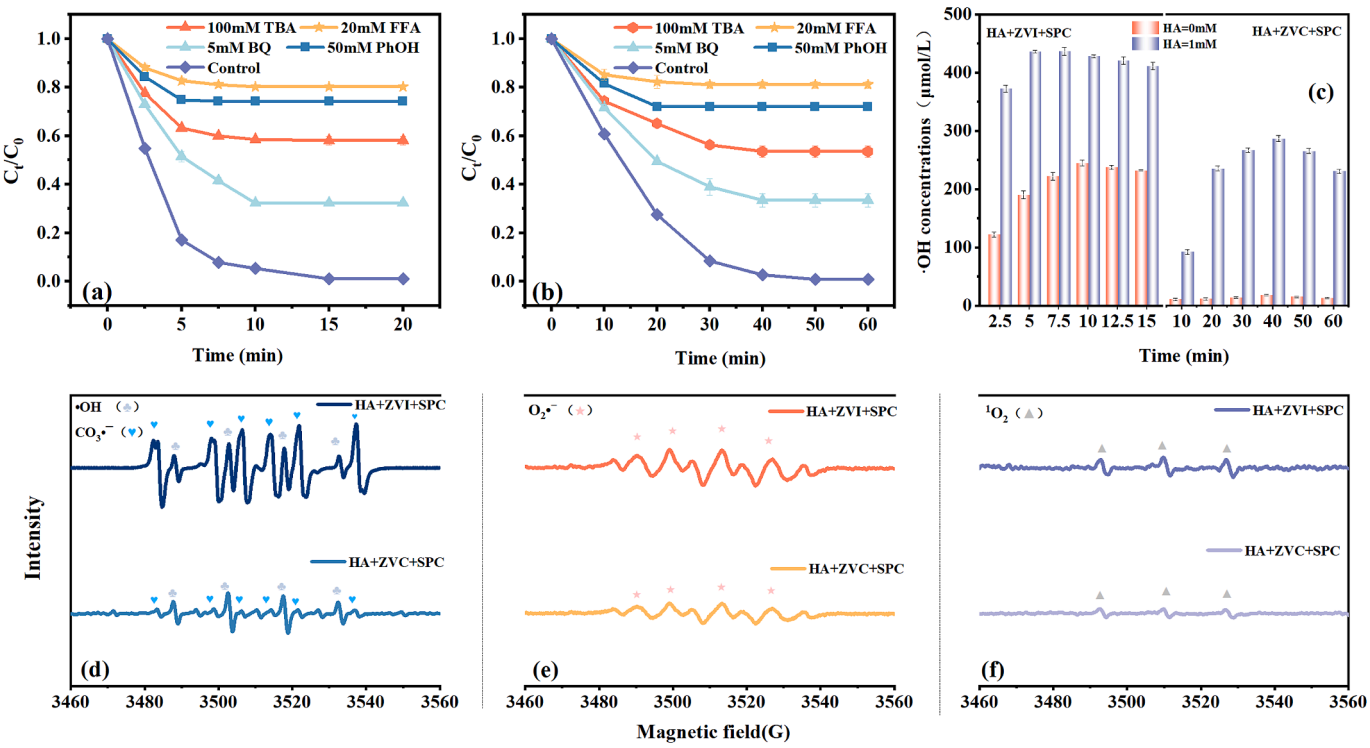

Fig. 3. Results of quenching experiments for (a) the HA/ZVI/SPC system; (b) the HA/ZVC/SPC system; (c) •*OH* concentration changes; (d), (e), (f) EPR spectra of HA/ZVM/SPC: (♥)DMPO−$CO_3^{\bullet-}$, (♠)DMPO−$^{\bullet}OH$, (★)DMPO − $O_2^{\bullet-}$and (▲)TEMP − $^1O_2$. Experimental conditions: $[ZVI]_0 = 0.05$ g/L, $[ZVC]_0 = 0.10$ g/L, $[SPC]_0 = 1$ mM, $[AZO]_0 = 10$ mg/L, $[HA]_0 = 1$ mM, $[pH]_0 = 3$.

oxidation process [17,37]. The effects of HCO_3^-, Cl^-, SO_4^{2-}, NO_2^- and humic acid on AZO degradation are discussed in detail in SI (Text S3, Fig. S5).

3.4. Mechanistic insights into the HA/ZVM/SPC processes

3.4.1. The identification of active species

In the two HA/ZVM/SPC systems, signals for $^{\bullet}OH$ (DMPO-$^{\bullet}OH$), $O_2^{\bullet-}$ (DMPO-$O_2^{\bullet-}$), $CO_3^{\bullet-}$ (DMPO-$CO_3^{\bullet-}$) and $^1O_2$ (TMPO-$^1O_2$) could be detected, at various signal intensities (Fig. 3d, e and f). During the degradation of AZO in the HA/ZVI/SPC system, signals could be clearly detected for $^{\bullet}OH$, $O_2^{\bullet-}$ and $CO_3^{\bullet-}$, while the signals of $^{\bullet}OH$, $O_2^{\bullet-}$ and $CO_3^{\bullet-}$ were much weaker in the HA/ZVC/SPC system. In contrast, $^1O_2$ signals were weak in both systems, indicating that $^1O_2$ production was generally low. A part of the $^{\bullet}OH$ is converted into $O_2^{\bullet-}$ and $^1O_2$ during the process by the chain reaction outlined in Equations (7)–(9) [38–41].

$$H_2O_2 + {}^{\bullet}OH \rightarrow H_2O + O_2^{\bullet-} \quad (7)$$

$$O_2^{\bullet-} + {}^{\bullet}OH \rightarrow {}^1O_2 + OH^- \quad (8)$$

$$O_2^{\bullet-} + 2H_2O \rightarrow H_2O_2 + {}^1O_2 + OH^- \quad (9)$$

The contribution of different radicals to AZO degradation in both systems was explored through quenching experiments, as illustrated in Fig. 3a and b. The quenching results for the two HA/ZVM/SPC systems were almost identical and therefore, the HA/ZVI/SPC system is discussed as an example. First, *tert*-butanol (TBA) was used to evaluate the contribution of $^{\bullet}OH$ ($k=(3.8–7.6) \times 10^8$ $M^{-1}s^{-1}$), with the addition of 100 mM tert-butanol causing AZO removal to decrease from 99.0 % to 42.0 %, indicating that $^{\bullet}OH$ production occurs through the conventional Fenton-like reaction process (Equations (10), (11)). In previous studies, it has been demonstrated that SPC can break down into carbonate ions and H_2O_2, which can further transform $^{\bullet}OH$ into other reactive oxygen species [6,42]. In order to further assess potential reactive oxygen species involved, scavengers of $CO_3^{\bullet-}$, $O_2^{\bullet-}$ and $^1O_2$ were chosen. Second, phenol (PhOH) was used to evaluate the contribution of $^{\bullet}OH$ and $CO_3^{\bullet-}$, showing that the removal of AZO was significantly reduced to 25.9 % with the addition of 50 mM phenol, with the difference in degradation efficiencies between the *tert*-butanol and phenol treated systems, confirming the presence of $CO_3^{\bullet-}$. Third, furfuryl alcohol (FFA) was added as a scavenger of $^1O_2$ and $^{\bullet}OH$, with 20 mM furfuryl alcohol found to reduce AZO removal to 19.9 %, while finally the addition of 5 mM benzoquinone (BQ) led to a reduction in AZO removal to 68.5 %, confirming that $O_2^{\bullet-}$ played a significant role in AZO degradation. These experimental results indicate that the HA/ZVI/SPC and HA/ZVC/SPC systems may both generate $^{\bullet}OH$, $CO_3^{\bullet-}$, $O_2^{\bullet-}$ and $^1O_2$, with the ranked contributions of these radical species being $^{\bullet}OH > O_2^{\bullet-} > {}^1O_2 > CO_3^{\bullet-}$.

The concentrations of $^{\bullet}OH$ in the degradation processes of all four systems, ZVI/SPC, ZVC/SPC, HA/ZVI/SPC and HA/ZVC/SPC, were monitored and compared. The amount of $^{\bullet}OH$ produced in HA/ZVI/SPC system was much higher than that in ZVI/SPC system, as illustrated in Fig. 3c, and the same phenomenon was also observed in HA/ZVC/SPC system. This further accounts for the promotion of AZO degradation by HA, in which the addition of HA can accelerate Fe^{2+}/Fe^{3+} or Cu^+/Cu^{2+} cycling, promoting the generation of reactive radicals. In the HA/ZVI/SPC system, $^{\bullet}OH$ generation rose to 436.5 μM after 15 min, and by the time the degradation process was complete, it had progressively dropped to 410.5 μM. The same phenomenon was observed in all other systems. This could be explained by the fact that $^{\bullet}OH$ interacted with HCO_3^-/CO_3^{2-} to form other reactive oxygen species during the reaction process, as given by Equations (12)–(18) [30].

$$Cu(I) + H_2O_2 \rightarrow Cu(II) + OH^- + {}^{\bullet}OH \quad (10)$$

$$Fe(II) + H_2O_2 \rightarrow Fe(III) + OH^- + {}^{\bullet}OH \quad (11)$$

$$^{\bullet}OH + CO_3^{2-} \rightarrow OH^- + CO_3^{\bullet-} \quad (12)$$

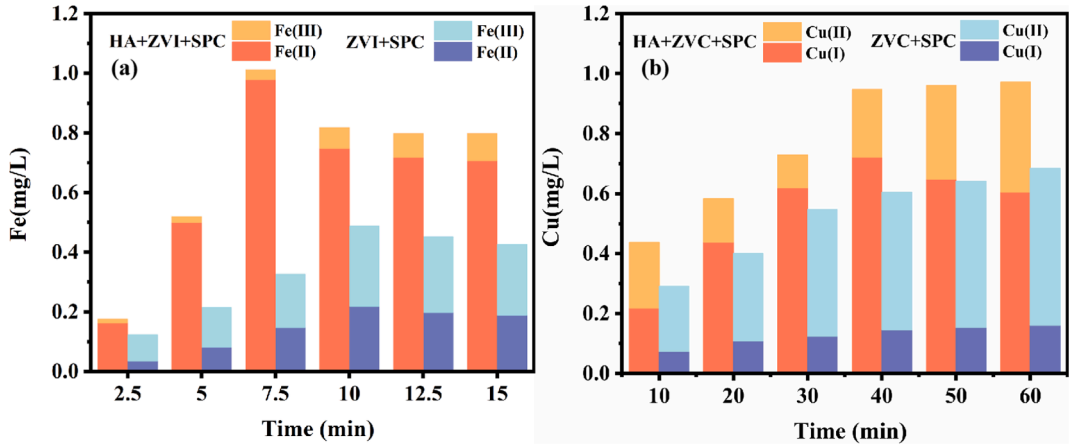

Fig. 4. (a) Variation in Fe ion concentration in the Fe-based system solution; (b) Variation in Cu ion concentration in the Cu-based system solution. Experimental conditions: $[ZVI]_0$ = 0.05 g/L, $[ZVC]_0$ = 0.10 g/L, $[SPC]_0$ = 1 mM, $[AZO]_0$ = 10 mg/L, $[HA]_0$ = 1 mM and $[pH]_0$ = 3.

$$^{\bullet}OH + HCO_3^- \rightarrow H_2O + CO_3^{\bullet-} \quad (13)$$

$$H_2O_2 + CO_3^{\bullet-} \rightarrow HCO_3^- + HO_2^{\bullet} \quad (14)$$

$$HO_2^{\bullet} \rightarrow H^+ + O_2^{\bullet-} \quad (15)$$

$$O_2^{\bullet-} + {}^{\bullet}OH \rightarrow {}^1O_2 + OH^- \quad (16)$$

$$HO_2^{\bullet} + O_2^{\bullet-} \rightarrow {}^1O_2 + HO_2^- \quad (17)$$

$$2O_2^{\bullet-} + 2H_2O \rightarrow {}^1O_2 + H_2O_2 + 2OH^- \quad (18)$$

3.4.2. *Function of carbonate ions*

In the two HA/ZVM/SPC systems, the function of carbonate ions was investigated during the evolution of reactive oxygen species. As the quenching effects observed in the two systems were similar, the ZVI system was used to compare the effects of ZVI catalysis by equal amounts of H_2O_2 and Na_2CO_3 with SPC components. The AZO degradation efficiency of the HA/ZVI/Na_2CO_3/H_2O_2 system was higher than that of the HA/ZVI/H_2O_2 process but slightly lower than that of the HA/ZVI/SPC process, due to the existence of trace CO_3^{2-} (SI, Fig. S6a). This phenomenon is likely due to alterations in the reactive oxygen species, which may play a buffering role, thereby enhancing the utilization efficiency of the low-dose oxidant [43]. Meanwhile, $CO_3^{\bullet-}$ can be transformed into $O_2^{\bullet-}$ as shown by Equations (19)-(20). The EPR spectra of HA/ZVI/H_2O_2 and HA/Na_2CO_3/ZVI/H_2O_2 processes were analyzed using DMPO as a trapping agent (SI, Fig. S6d, e, f). Results showed that signals for $CO_3^{\bullet-}$ radicals were obtained in the HA/Na_2CO_3/ZVI/H_2O_2 system, which were weaker than the SPC system signals, confirming that a portion of $^{\bullet}OH$ was converted to $CO_3^{\bullet-}$, although the oxidation mechanism of the HA/ZVI/SPC process could not be established simply based on theoretical calculations assuming the addition of equal amounts of H_2O_2 and Na_2CO_3.

As shown in Fig. S6b (SI), AZO removal in the HA/Na_2CO_3/ZVI/H_2O_2 system reached 45.4 %, 32.1 %, 60.2 % and 26.8 % with the addition of *tert*-butanol, furfuryl alcohol, benzoquinone and phenol, respectively, indicating that $^{\bullet}OH$, $CO_3^{\bullet-}$, $O_2^{\bullet-}$ and $^1O_2$ coexisted within the system. This demonstrates that the presence of CO_3^{2-} promoted the generation of other reactive oxygen species. The relationships between $^{\bullet}OH$ concentration, the AZO removal rate and carbonate ion concentration were explored. In the HA/Na_2CO_3/ZVI/H_2O_2 system, when the carbonate ion concentration was raised from 0 to 1.0, 2.0, 3.0 and 5.0 mM, the rate of AZO removal changed from 88.3 % to 93.2 %, 74.3 %, 57.7 % and 44.7 %, while the final $^{\bullet}OH$ concentration decreased from 462.3 μM to 422.5, 351.1, 268.7 and 102.5 μM (Fig. S6c). Surplus carbonate ions act as scavengers for $^{\bullet}OH$ and $O_2^{\bullet-}$ [44]. Therefore, it can be concluded that the produced $^{\bullet}OH$ is crucial to the system because it forms other reactive oxygen species with carbonate ions in a sequence of chain reactions, which helps to partially degrade AZO.

$$CO_3^{\bullet-} + H_2O_2 \rightarrow HO_2^{\bullet} + HCO_3^- \quad (19)$$

$$HO_2^{\bullet} \rightarrow H^+ + O_2^{\bullet-} \quad (20)$$

3.4.3. *Transformation of metal ions within the system*

The concentrations of dissolved Fe^{3+}, Fe^{2+}, Cu^{2+}, and Cu^+ were measured during the reaction in order to assess the contribution of Fe and Cu ion leaching by ZVI and ZVC to SPC activation within the system. According to Fig. 4a, in the ZVI/SPC system, the concentration of total Fe (including Fe^{3+} and Fe^{2+}) gradually increased to 0.48 mg/L with ongoing reaction time, then gradually decreased to 0.43 mg/L, with Fe^{3+} accounting for a little more. As shown in Eq. (21), ZVI can partially reduce Fe^{3+} to Fe^{2+}, with the dissolved Fe^{2+} and Fe^{2+} generated on the surface of ZVI also able to activate SPC for the decomposition of organic pollutants. After the addition of HA, Fe^{2+} concentration increased rapidly (from 0.16 mg/L to 0.97 mg/L during the first 7.5 min) and remained at a high level and accounted for most of the total iron content throughout the reaction process. The concentration of Fe^{2+} increased quickly in the presence of HA, causing the Fe^{3+} generated in the solution to be continuously reduced to Fe^{2+}. However, the continuous consumption of HA and Fe^{2+} during the reaction process, resulted in a slowing of the ZVI corrosion rate, with the conversion of Fe^{2+} generated by Fe^{3+} reduction, back to Fe^{3+} during SPC activation. In the later stages of the reaction, the concentration of Fe^{3+} steadily increased while the concentration of Fe^{2+} gradually declined (to 0.70 mg/L). Combined with the observed decrease in removal rate, this indicates that the extra Fe^{2+} generated in the early stages of the reaction competed with pollutants for free radicals Eq. (22). The gradual decrease in total Fe content in the Fe-based reaction was attributed to the observed increase in pH and the precipitation of Fe ions due to SPC during the reaction, causing the Fe sludge to precipitate out of the water.

$$Fe^{3+} + Fe^0 \rightarrow Fe^{2+} \quad (21)$$

$$Fe^{2+} + {}^{\bullet}OH \rightarrow Fe^{3+} + OH^- \quad (22)$$

Cu leaching from the ZVC/SPC system is shown in Fig. 4b, where the Cu^+ ion concentration remained at a low level (maximum 0.16 mg/L) and AZO removal was low (10 %), presumably due to insufficient Cu^+ availability for SPC activation to produce reactive oxygen species. The final total copper concentration in the ZVC/SPC system (0.68 mg/L) was lower than in the HA/ZVC/SPC system (0.97 mg/L). After the addition

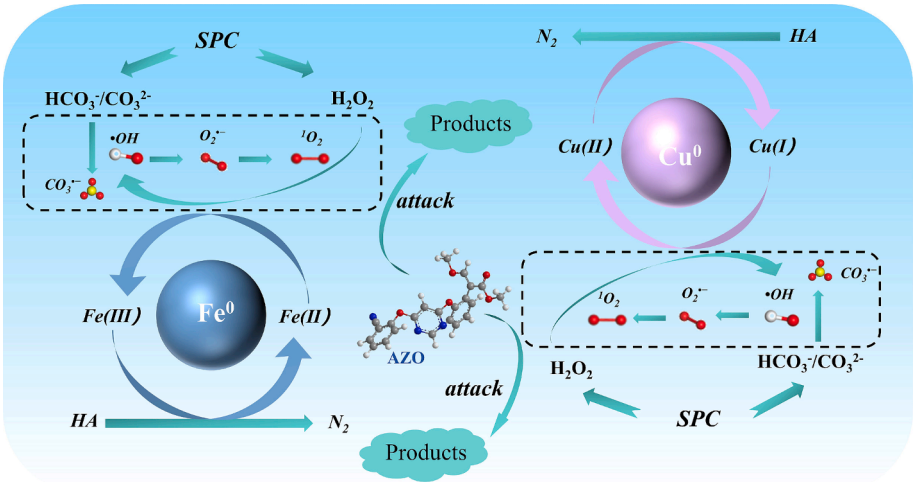

Fig. 5. Schematic diagram of the proposed reaction mechanism of AZO degradation by HA/ZVM/SPC processes.

of HA, the concentration of Cu^{+} in the system increased rapidly to 0.72 mg/L within the first 40 min and then decreased to 0.6 mg/L, accounting for more than 60 % of the total Cu concentration throughout the whole process. This provided a large number of low-valent ions for SPC activation, promoting the generation of reactive oxygen species and improving the rate of AZO removal. Compared with the Fe-based system, the total amount of metal in the Cu-based system did not gradually decrease in later stages of the reaction, mainly because Cu ions are not as affected by pH as Fe ions [45].

These findings unequivocally show that the regeneration of Cu^{+} and Fe^{2+} in solution was made possible by the addition of HA. In light of the aforementioned conclusions, a possible mechanism for SPC activation by HA-enhanced ZVI and ZVC is proposed in Fig. 5. First, the corrosion of ZVI and ZVC generates Fe^{2+} and Cu^{+} ions [46]. Then, Fe^{2+} and Cu^{+} can directly activate the H_2O_2 generated by SPC to produce $^{\bullet}OH$ and Fe^{3+} or Cu^{2+}. Subsequently, the available $^{\bullet}OH$ is then mostly transformed into other reactive oxygen species, such as $CO_3^{\bullet-}$, $O_2^{\bullet-}$ and $^1O_2$ through a chain reaction in the presence of carbonate ions, and these reactive oxygen species react with and degrade contaminants [30]. HA directly reacts with Fe^{3+} and Cu^{2+} to generate Fe^{2+} and Cu^{+}, maintaining the activity of metal ions in the reaction and thus leading to a high reaction efficiency. In addition, HA reacts with hydrogen peroxide to generate hydroxyl radicals and other reaction intermediates, as shown in Eq. (23) [37].

$$NH_2OH + H_2O_2 \rightarrow {}^{\bullet}OH + H_2O + NHOH \quad (23)$$

3.4.4. Characterization of catalysts before and after reaction

The XPS analysis results of ZVI before and after usage in the AZO degradation reaction are displayed in Fig. 6a in order to further analyze the mechanism of AZO degradation in the HA/ZVI/SPC and HA/ZVC/SPC systems. The characteristic signals of Fe^{2+} were observed at 710.4 eV and 723.6 eV with Fe $2p_{3/2}$ and Fe $2p_{1/2}$, while another characteristic peak located at 712.8 eV could indicate the presence of Fe^{3+} in ZVI [47]. In addition, the signal detected at a binding energy of 707.0 eV was assigned to Fe^{0} [21,48], while that at 718.0 eV was attributed to a broad satellite peak of Fe^{3+}, with these results indicating the presence of multivalent Fe. The relative proportions of Fe^{0}, Fe^{2+} and Fe^{3+} after use in the ZVI/SPC system were 0 %, 41.3 % and 58.7 %, respectively, while in the HA/ZVI/SPC system, the relative proportions of Fe^{0}, Fe^{2+} and Fe^{3+} after the reaction were 11.2 %, 42.2 % and 46.6 %, respectively. Compared with the ZVI/SPC system, the proportion of Fe^{3+} was lower and the proportion of Fe^{2+} and Fe^{0} was higher in the HA/ZVI/SPC system, and a thicker and more compact oxidized layer was present on the surface of ZVI after the ZVI/SPC system reaction, indicating that HA slowed down the surface passivation of ZVI and promoted the conversion of Fe^{3+} to Fe^{2+}.

The results of XPS analysis pre- and post-use in the ZVC reaction (Fig. 6b) exhibited weak satellite peaks, indicating the presence of trace Cu^{2+} oxidation [49]. The peaks located at 933.6, 944.6, 953.4 and 960.2 eV were related to Cu^{2+} oxidation [50]. Only a small amount of Cu^{2+} was present before and after the reaction, due to Cu being more stable than Fe. The characteristic peaks at 932.8 eV and 952.5 eV indicate the presence of reduced Cu (Cu^{0}/Cu^{+}). However, the binding energy difference between Cu^{0} and Cu^{+} is very small, so it is difficult to distinguish them, with neither of them exhibiting satellite peaks [51]. In addition, the peaks of the reduced Cu species in the HA/ZVC/SPC system shifted slightly to higher binding energies of 933 eV and 952.8 eV and are slightly wider than those of ZVC/SPC, implying that the valence transition between Cu^{2+} and Cu^{+} on the surface of zero-valent copper was facilitated by HA during AZO removal [51].

Metal hydroxyl oxygen (M−OH) or lattice oxygen (Olo), surface adsorbed oxygen (Oao) or oxygen vacancy (Ovo), and surface hydroxyl oxygen (Oso) were identified as the sources of the peaks at 530.1, 531.7, and 533.1 eV, respectively [52]. In the ZVI/SPC system (Fig. 6c), the proportions of M−OH or Olo, Oao or Ovo, and Oso functional groups were 43.9 %, 38.1 % and 18 %, respectively, while after the addition of HA, they were 40 %, 41.1 % and 20.9 %, respectively. In used ZVI after the ZVI/SPC system reaction, the lattice oxygen content accounted for the largest proportion, indicating that at this time, ZVI surface structures were mainly iron oxides, with a stable crystal structure, inhibiting the activity of the catalyst. After the addition of HA, the proportion of surface hydroxyl oxygen compounds gradually increased and structurally stable oxides decreased, which was conducive to achieving a maximum ZVI activity. Furthermore, the proportion of surface hydroxylation increased while crystalline oxides gradually decreased, resulting in high activity and more effective pollutant removal performance [53,54]. In the ZVC/SPC system (Fig. 6d), the proportions of M−OH or Olo, Oao or Ovo, and Oso functional groups on the surface of ZVC were 27 %, 37.5 % and 35.5 %, respectively, with the addition of HA resulting in proportions of 22.8 %, 40.6 % and 36.6 %, respectively. Similar to the trend shown for ZVI, the addition of HA caused the proportion of lattice oxygen to decrease and the proportion of surface hydroxyl oxygen to increase.

The XRD spectra of ZVI and ZVC before and after use as a catalyst were compared (Fig. 6e and f), showing that no oxide diffraction peaks were present in the XRD spectra of ZVI and ZVC before or after use. This indicates that ZVI and ZVC were not over-oxidized, with the oxidized layer accounting for no more than 5 % of the total content, while also showing that ZVC and ZVI exhibited better stability. However, the elemental diffraction peak signals of ZVI and ZVC were slightly

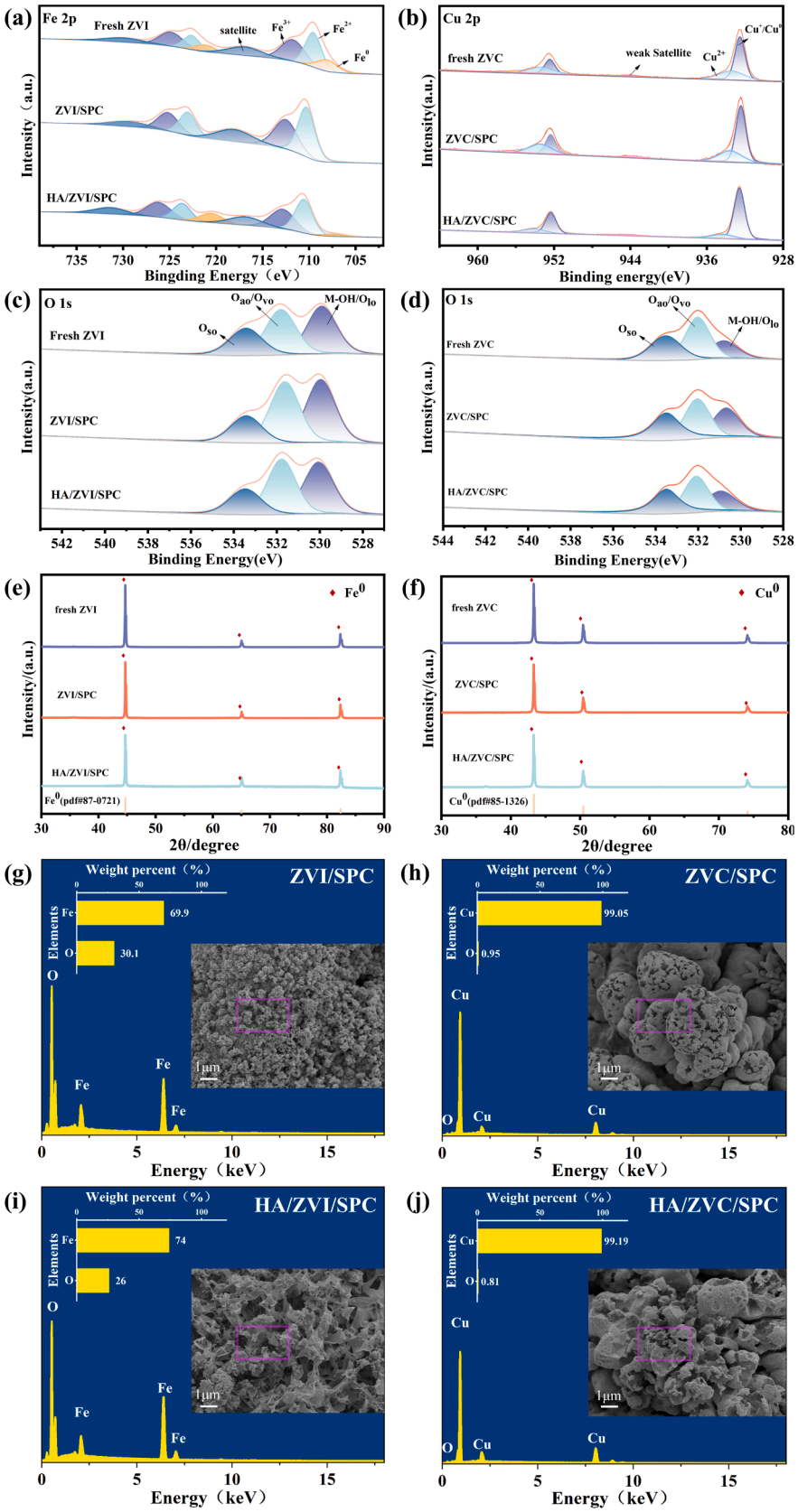

Fig. 6. (a) Fe 2p; (c) O 1 s XPS spectra and (e) XRD spectra of pristine ZVI, ZVI particles after use in the ZVI/SPC system and ZVI particles after use in the HA/ZVI/SPC system; (b) Cu 2p; (d) O 1 s XPS spectra and (f) XRD of pristine ZVC, ZVC particles after reaction in ZVC/SPC system and ZVC particles after reaction in HA/ZVC/SPC system; (g) SEM and EDS of ZVI particles after use in the ZVI/SPC system; (h) SEM and EDS of ZVC particles after use in the ZVC/SPC system; (i) SEM and EDS of ZVI particles after use in HA/ZVI/SPC system; (j) SEM and EDS of ZVC particles after use in the HA/ZVC/SPC system.

Table 1
Fukui index of AZO.

Atom	q(N)	q(N + 1)	q(N-1)	f^-	f^+	f^0
C 1	−0.0407	−0.0661	−0.0242	0.0166	0.0254	0.021
C 2	0.0869	0.063	0.1372	0.0504	0.0238	0.0371
C 3	0.0042	−0.0408	0.0634	0.0592	0.045	0.0521
C 4	−0.018	−0.0632	0.0231	0.0412	0.0451	0.0432
C 5	−0.0357	−0.072	0.0506	0.0864	0.0362	0.0613
C 6	−0.0217	−0.0838	0.0442	0.066	0.0621	0.064
H 7	0.0422	0.0302	0.0514	0.0092	0.012	0.0106
H 8	0.0548	0.0283	0.0891	0.0343	0.0265	0.0304
H 9	0.0479	0.0223	0.0912	0.0432	0.0257	0.0345
H 10	0.0495	0.0187	0.0838	0.0343	0.0307	0.0325
C 11	0.0638	0.0267	0.1017	0.0379	0.037	0.0375
N 12	−0.2111	−0.2984	−0.0851	0.126	0.0874	0.1067
O 13	−0.1042	−0.117	−0.0666	0.0375	0.0129	0.0252
C 14	0.1441	0.1312	0.1615	0.0174	0.0129	0.0151
C 15	−0.0698	−0.0918	−0.0449	0.0249	0.0221	0.0235
C 16	0.089	0.0551	0.116	0.027	0.0339	0.0305
C 17	0.1403	0.1268	0.1518	0.0115	0.0135	0.0125
H 18	0.0571	0.0422	0.0789	0.0218	0.0149	0.0184
H 19	0.0505	0.031	0.0765	0.026	0.0196	0.0228
N 20	−0.1804	−0.1853	−0.1396	0.0409	0.0048	0.0228
N 21	−0.1724	−0.2012	−0.1361	0.0363	0.0288	0.0326
C 22	−0.0342	−0.0574	0.0726	0.1068	0.0232	0.065
C 23	−0.0443	−0.065	0.0579	0.1022	0.0207	0.0615
C 24	−0.0343	−0.0422	0.0033	0.0376	0.0079	0.0227
C 25	−0.0121	−0.0077	0.0537	0.0657	−0.0044	0.0307
C 26	0.0756	0.0733	0.1482	0.0726	0.0023	0.0375
C 27	−0.0462	−0.0592	0.0025	0.0487	0.013	0.0309
H 28	0.0444	0.0284	0.098	0.0536	0.016	0.0348
H 29	0.0419	0.0266	0.0943	0.0525	0.0152	0.0339
H 30	0.0398	0.033	0.0727	0.0329	0.0068	0.0198
H 31	0.0483	0.0371	0.0892	0.0409	0.0112	0.026
O 32	−0.1096	−0.1206	−0.0532	0.0563	0.011	0.0337
C 33	−0.054	−0.0759	0.0089	0.0628	0.0219	0.0424
C 34	0.0667	0.0234	0.1249	0.0581	0.0433	0.0507
H 35	0.0465	0.0331	0.0736	0.0271	0.0134	0.0203
O 36	−0.0995	−0.1207	−0.0353	0.0642	0.0212	0.0427
C 37	0.0151	0.0051	0.0392	0.0242	0.0099	0.017
H 38	0.0428	0.028	0.0734	0.0306	0.0148	0.0227
H 39	0.0549	0.0406	0.0825	0.0276	0.0144	0.021
H 40	0.0427	0.0408	0.0597	0.017	0.0019	0.0094
C 41	0.189	0.1579	0.2056	0.0166	0.0312	0.0239
O 42	−0.2752	−0.3005	−0.2129	0.0622	0.0253	0.0438
O 43	−0.113	−0.1331	−0.0948	0.0182	0.0201	0.0191
C 44	0.0067	−0.003	0.0244	0.0177	0.0097	0.0137
H 45	0.0402	0.0357	0.0509	0.0107	0.0045	0.0076
H 46	0.0487	0.035	0.071	0.0224	0.0136	0.018
H 47	0.0427	0.0313	0.0656	0.0228	0.0115	0.0172

weakened after use, indicating that the catalyst structure was degraded due to oxidant activation. While a minor loss of catalytic performance was observed throughout the process, the overall activity changed very little, confirming that the surface lattice structure of the catalysts was relatively stable [52,55].

The morphology and structural features of ZVI and ZVC pre- and post-use in the reaction were characterized. As demonstrated by the SEM image of ZVI in Fig. S1g (SI), the surface of ZVI was relatively smooth before the reaction, becoming significantly rougher after use in the ZVI/SPC reaction (Fig. 6g), with a large number of oxide particles and obvious corrosion traces. After the addition of HA (Fig. 6i), the surface of ZVI became rougher but the oxide particles were significantly reduced. This indicates that HA can effectively slow down the deposition of hydroxides or Fe oxides on the surface of ZVI. As a result, more ZVI surface active sites remain exposed and therefore maintain a high activity, which is in line with the results of XPS analysis. As demonstrated by the SEM image of ZVC in Fig. S1h (SI), before use, the ZVC exhibited an irregular cluster structure composed of many spherical particles of different particle sizes, providing a large specific surface area and very few surface oxides, which was favorable for the interfacial reaction between ZVC and other substances. After the ZVC/SPC and HA/ZVC/SPC system reactions, the surfaces became rough and uneven due to corrosion. Compared with the ZVC/SPC system (Fig. 6h), ZVC corrosion in the HA/ZVC/SPC system was significantly enhanced (Fig. 6j), presumably due to the reaction between HA and Cu^{2+} on the surface of ZVC, releasing H^+, as shown in Eq. (24). Compared to ZVI after use in the reaction, the surface of used ZVC contained almost no oxides, making it more likely to react with acids causing serious corrosion on the surface of ZVC.

$$NH_2OH + Cu(II) \rightarrow \frac{1}{2}N_2 + H_2O + Cu(I) + H^+ \quad (24)$$

3.5. Potential for practical applications

Reusability and stability of a catalytic material are the main criteria used to evaluate its suitability and effectiveness. Consequently, the two HA/ZVM/SPC systems were used to examine the recyclability of the ZVM catalyst and the findings are displayed in Fig. S7 (SI).

The degradation capability of both ZVM catalysts exhibited a slowly decreasing trend with increasing cycles of use. In particular, both catalysts exhibited maximum degradation efficiencies when used for the first time and after four cycles of reuse. The rate of AZO removal still remained at a high level of more than 90 %. After four cycles of reuse,

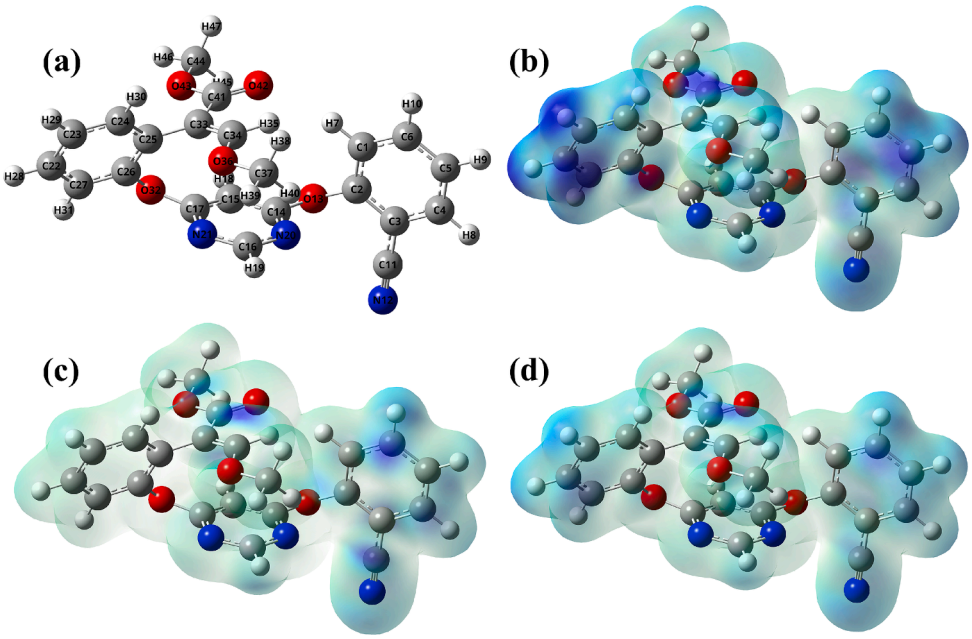

Fig. 7. (a) AZO structure optimization; The Fukui function mapped electron density *iso*-surface (ρ = 0.01 a.u.): (b) f, (c) f^{+}, (d) f^{0}. The dark blue on the *iso*-surface denotes a more positive Fukui function value. (For interpretation of the references to color in this figure legend, the reader is referred to the web version of this article.)

the rate of AZO removal was 93.4 % in the HA/ZVI/SPC system, while it was 91.1 % in the HA/ZVC/SPC system. These findings further indicate that the ZVM catalyst was able to maintain high activity and stable degradation performance even after multiple cycles of reuse. In addition, surface analysis of the catalyst showed that ZVM had a special microstructure and active sites, which may be a key factor in the stability of ZVM, allowing it to maintain a good degradation performance even after repeated cycles of use. During recycling, the surface of the catalyst material was able to effectively maintain the key structural features, ensuring its continual high efficiency, activity and performance.

Second, the total leaching amounts of ZVI and ZVC in both HA/ZVM/SPC systems were monitored for 72 h. As shown in Fig. S8, at the 72nd hour, the total iron and copper contents in the system reached 7.15 mg/L and 5.98 mg/L, respectively. Therefore, the metal catalyst should be recovered as soon as possible after the reaction to reduce the pollution of metal ions in the environment.

To further evaluate the performance of the two HA/ZVM/SPC systems, the degradation experiments of six emerging pollutants (AZO, SMX, TC, CiFX, IBU and TCP) were carried out under the optimal conditions ($[ZVI]_0 = 0.05$ g/L, $[ZVC]_0 = 0.10$ g/L, $[SPC]_0 = 1$ mM, $[HA]_0 = 1$ mM, $[pH]_0 = 3$ and $[poll]_0 = 10$ mg/L.), and the experimental results are shown in Fig. S9. The two HA/ZVM/SPC systems exhibited good degradation performance for various pollutants. In HA/ZVI/SPC system, the degradation rate of all six pollutants reached more than 90 % within 15 min, and the degradation rate of four pollutants reached more than 99 %. In HA/ZVC/SPC system, the degradation rate of all six pollutants reached more than 92 % within 50 min, and the degradation rate of four pollutants also reached more than 99 %. Furthermore, the removal rates of AZO with different concentrations in the two HA/ZVM/SPC systems were evaluated, as shown in Text S4 and Fig. S10, SI. The total organic carbon (TOC) removal was determined to evaluate the degree of mineralization in the treated AZO samples. The results shown in Fig. S11 clearly prove that the mineralization rate of AZO was above 25 % in both HA/ZVM/SPC systems. The above results show that HA/ZVM/SPC system has good environmental purification potential.

In order to determine whether the addition of HA causes the total nitrogen concentration in the system to be too high, the change in total nitrogen concentration in the system was detected. In HA/ZVI/SPC system (Fig. S12), the total nitrogen concentration decreased from 8.46 mg/L to 7.54 mg/L within 15 min. In HA/ZVC/SPC system, the concentration of total nitrogen decreased from 8.42 mg/L to 6.99 mg/L within 50 min. The decrease in total nitrogen in this experiment implies that part of HA was converted into gaseous nitrogen.

3.6. AZO degradation intermediates and their toxicity evaluation

The reactivity of a compound may often be predicted using the energies of its lowest unoccupied molecular orbital (LUMO) and highest occupied molecular orbital (HOMO). Gauss software was used to build block AZO and describe its LUMO and HOMO to illustrate the electron gain and loss ability. While the HOMO region is often used to describe the ease of electron escape, the HOMO region of AZO is easily attacked by the electrophilic substances such as $O_2^{\bullet-}$ and $^1O_2$ in the system (Fig. S13b, SI) [46]. In addition, the Fukui index is an important parameter as it reveals the difficulty of a molecular reaction. Studying the intermolecular electrostatic interactions also involves considering the electrostatic potential distribution (ESP) on the surface of the molecule. The distribution of the electrostatic potential of the AZO molecule was slightly different, presenting a color sequence from blue (indicating a positive potential) to red (indicating a negative potential). The electron-rich functional groups were attacked by electrophilic reactive oxygen species, which are shown in a red color in the calculated results [56,57]. The negative potential portion of AZO was mainly distributed on the carboxyl group and the cyano group (Fig. S13a, SI), which were the main electron-rich functional groups susceptible to attack by electrophilic reactive oxygen species.

In addition, Multiwfn software was utilized to calculate the electrophilic attack index (f⁻), nucleophilic attack index (f^{+}) and radical attack index (f^{0}) of the AZO molecule, as shown in Table 1, Fig. 7, with a higher index value indicating a higher possibility that the AZO molecule would be attacked by the corresponding type of substance.

As $^1O_2$ is a non-radical electrophilic reagent, its possible attack sites were evaluated using f⁻, with results showing that N12, C5, C22, C23, C25, O36 and O42 were most reactive on AZO, but due to their spatial distribution (located within the benzene ring) and subsequent spatial

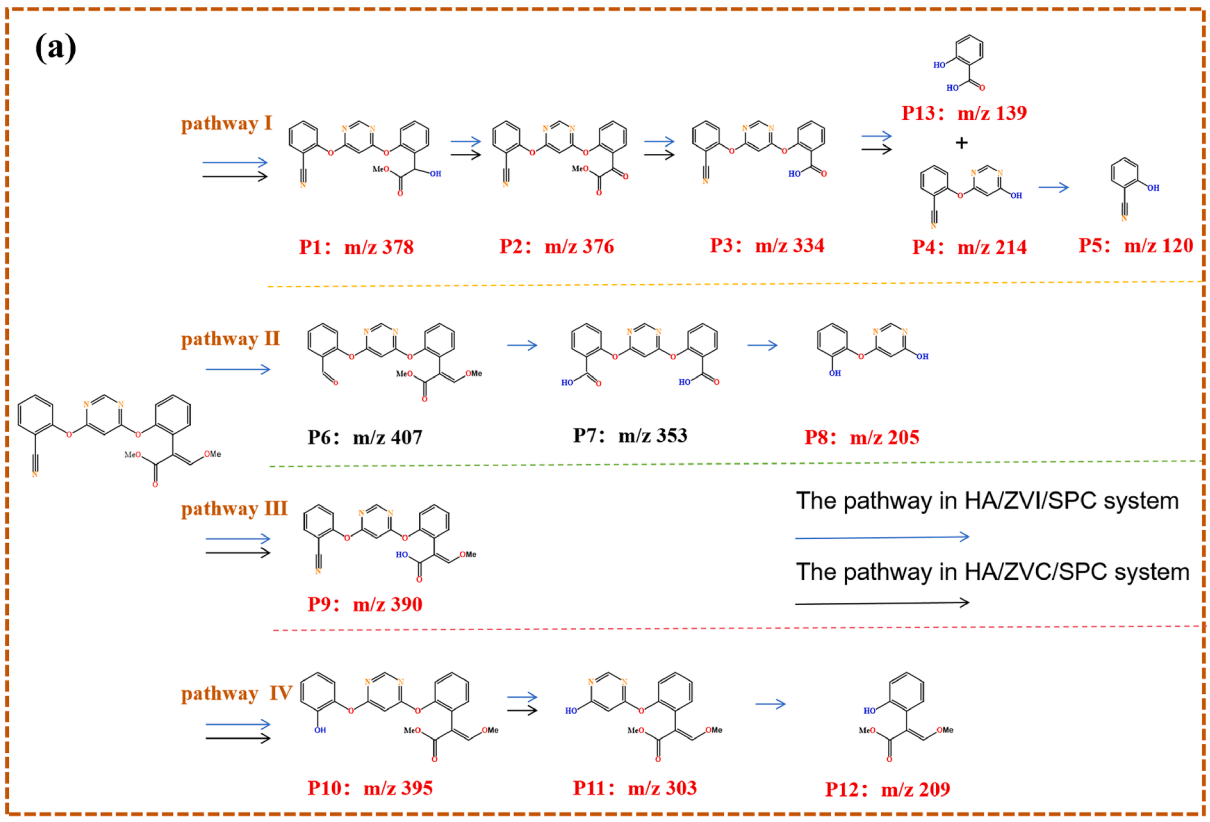

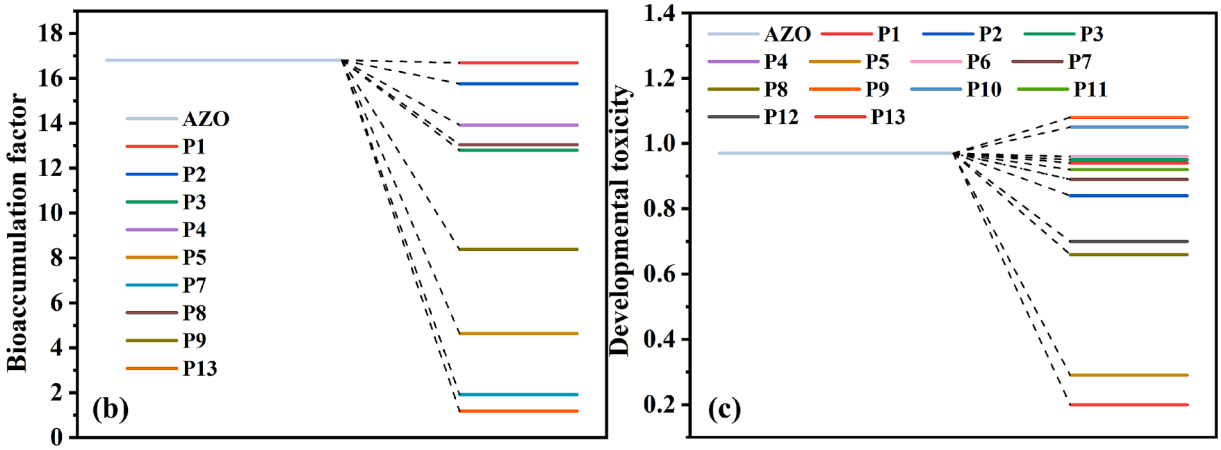

Fig. 8. Proposed pathway for AZO degradation by: (a) the HA/ZVI/SPC and the HA/ZVC/SPC processes; (b) bioaccumulation factors and (c) developmental toxicity of AZO and its possible degradation intermediates.

resistance, C5, C22, C23 and C25 do not easily react during oxidation [57]. In general, the benzene ring in organic matter is not usually oxidized directly, but by the electrophilic addition reaction of the •OH radical with phenyl [46].

The larger f^0 values of N12, C5, C6, C22, C23, C34, O36 and O42 indicate that these sites were more susceptible to free radical attack. In particular, N12, O36 and O42 atoms had higher f^- and f^0 values, indicating that they are highly susceptible to reactions with both electrophilic reagents and free radicals [12]. Among these, C34 was susceptible to oxidative reactions, although C5, C6, C22 and C23 had high Fukui index values and theoretically should all be susceptible to attack. However, free radical attack is more difficult due to the saturation of sites and active site resistance. In addition, sites C3, C4, C6 and N12 exhibited large f^+ values, although C4 and C6 atoms found it difficult to react with nucleophilic reagents due to spatial site resistance and bond saturation. In contrast, N12 and C3 were susceptible to nucleophilic reactions, leading to the occurrence of carbon–carbon bond breakage and nucleophilic substitution reactions.

The AZO degradation intermediates formed in the two HA/ZVM/SPC systems were deduced from the results of DFT theoretical calculations, with the possible intermediates proposed based on the theoretical calculations (Table S2, Fig. S14 and S15, SI) and subsequently, the possible degradation pathways were deduced (Fig. 8a). The detected HA/ZVI/SPC intermediates were P1: $C_{20}H_{15}N_3O_5$, P2: $C_{20}H_{13}N_3O_5$, P3: $C_{18}H_{11}N_3O_4$, P4: $C_{11}H_7N_3O_2$, P5: C_7H_5NO, P8: $C_{10}H_8N_2O_3$, P9: $C_{21}H_{15}N_3O_5$, P10: $C_{21}H_{18}N_2O_6$, P11: $C_{15}H_{14}N_2O_5$ and P12: $C_{11}H_{12}O_4$.

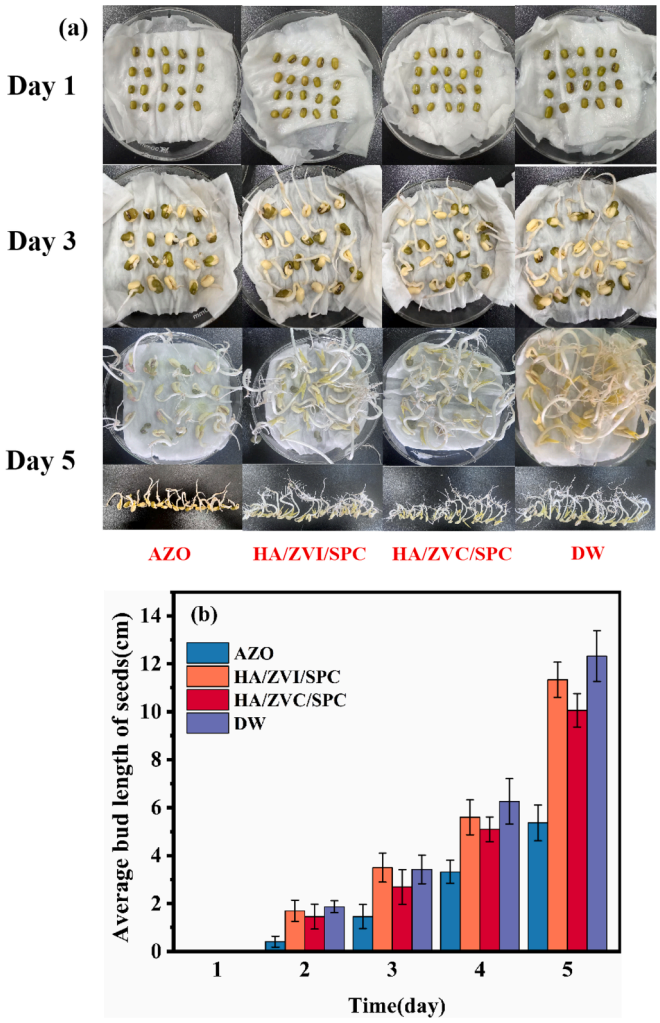

Fig. 9. (a) Seed germination photographs; (b) Average bud length of seeds. Experimental conditions: $[ZVI]_0$ = 0.05 g/L, $[ZVC]_0$ = 0.10 g/L, $[SPC]_0$ = 1 mM, $[AZO]_0$ = 10 mg/L, $[HA]_0$ = 1 mM, $[pH]_0$ = 3.

The detected HA/ZVC/SPC intermediates were P1: $C_{20}H_{15}N_3O_5$, P2: $C_{20}H_{13}N_3O_5$, P3: $C_{18}H_{11}N_3O_4$, P4: $C_{11}H_7N_3O_2$, P9: $C_{21}H_{15}N_3O_5$, P10: $C_{21}H_{18}N_2O_6$, P11: $C_{15}H_{14}N_2O_5$ and P13: $C_{11}H_{12}O_4$. Due to the differences in the reaction process between free radicals and organic matter in each of the systems, the AZO intermediate products may differ, although the degradation pathways of the two HA/ZVM/SPC systems were generally similar.

The pathway I process was utilized in both systems, in which the double bond of acrylate was first converted to the P1 enol-type metabolite by oxidative cleavage, followed by further oxidation to form the P3 benzoic acid-type metabolite through successive hydroxylation processes [16]. Subsequently, P4 and P13 intermediates were formed under $^{\bullet}OH$ attack, with P4 further degraded to P5 in the HA/ZVI/SPC system.

The pathway II degradation process occurred in the HA/ZVI/SPC system, in which the nitrile group is hydrolyzed to form its corresponding aldehyde structure (P6), which is then further oxidized to form P7, followed by a hydroxylation reaction to produce the P8 product [16]. The P8 product was detected, supporting this theoretical explanation.

Both HA/ZVI/SPC and HA/ZVC/SPC systems underwent pathway III and IV degradation processes, in which carboxylic acids are formed (P9) through methyl ester hydrolysis or dealkylation reactions [3]. Attack by reactive oxygen species in both systems resulted in the generation of P10 products followed by hydroxylation to produce P11 products, although in the HA/ZVI/SPC system, P11 products were further degraded to P12 products.

Additionally, the T.E.S.T. approach was used to predict the developmental toxicity and bioaccumulation factors of AZO and its breakdown products. Only the bioaccumulation factors of P6, P10, P11, and P12 could not be predicted out of all the intermediates evaluated. The AZO intermediates all demonstrated a decrease in bioaccumulation compared to pristine AZO, as seen in Fig. 8b, suggesting that AZO had a high bioaccumulation potential, although its intermediates were relatively less likely to accumulate in organisms, reducing their potential adverse effects. The capacity for AZO and its intermediate compounds to cause adverse effects on human or animal development was further evaluated in terms of developmental toxicity (Fig. 8c). Results showed that most of the AZO intermediates exhibited reduced developmental toxicity compared to the AZO parent compound, except for P9 and P10, with P5 and P13 in particular exhibiting a very low risk of developmental toxicity. In summary, these toxicity predictions highlight the important issue that AZO breakdown is accompanied by the production of toxic intermediates. Although the two HA/ZVM/SPC processes can reduce the toxicity of most AZO intermediates by forming less toxic decomposition products, some highly toxic intermediates remained, suggesting that further studies are needed to establish methods to reduce the toxicity of degradation products.

In order to further evaluate the toxicity of the solution treated with HA/ZVM/SPC, mung bean seeds were germinated in deionized water (DW), untreated AZO solution, and AZO solution treated with HA/ZVI/SPC and HA/ZVC/SPC. The planting date was set at 5 days. The germination photos and average bud length of seeds cultured in different water bodies for 1–5 days are shown in Fig. 9a and b. On the fifth day, the bud lengths of DW, untreated AZO, HA/ZVI/SPC and HA/ZVC/SPC groups were 12.3, 5.3, 11.3 and 10.0 cm, respectively. Obviously, the growth of bean sprouts in untreated AZO group was significantly inhibited, and both growth and bud length were significantly lower than those in treated AZO group and control group, which indicated that untreated AZO pesticide wastewater might have a certain toxic effect on organisms. At the same time, the growth degree of bean sprouts in HA/ZVI/SPC and HA/ZVC/SPC solutions was slightly lower than that in DW group, which may be due to the toxicity caused by the accumulation of intermediate products and iron/copper. This shows that HA/ZVM/SPC significantly reduced the biotoxicity of AZO, demonstrating its environmental-friendly characteristics and great practical application potential.

4. Conclusion

In this study, ZVI and ZVC were used as SPC activators to effectively degrade AZO in the presence of HA. Following the addition of HA to the system, the rate of AZO removal by the ZVI/SPC system increased from 42.7 % to 99.0 % within the first 15 min of treatment when pH = 3. In contrast, the rate of AZO removal by the ZVC/SPC system increased from 9.9 % to 99.1 % within the first 50 min of treatment when pH = 3. It is worth noting that when pH = 9, the removal rate of AZO by HA/ZVC/SPC system was still as high as 85.5 %. Therefore, the HA/ZVI/SPC system was more efficient in the removal of AZO, while the HA/ZVC/SPC system had a wider applicable pH range. The lower the pH, the higher the removal rate of AZO. However, pH lower than 3 is not suitable for real water treatment. The concentrations of Fe^{2+} and Cu^{+} in the solution increased with increase in initial HA concentration.

The presence of different reactive oxygen species in the two HA/ZVM/SPC systems was verified by quenching experiments and EPR testing, and their relative contribution rates were in the order: $^{\bullet}OH > O_2^{\bullet-} > {}^1O_2 > CO_3^{\bullet-}$. Using the $^{\bullet}OH$ probe method, it was shown that more $^{\bullet}OH$ was generated within the system in the presence of HA, thus promoting the removal of AZO. SPC contains trace amount of CO_3^{2-}. It has been shown previously that $^{\bullet}OH$ reacts with trace amounts of CO_3^{2-}

to generate other reactive oxygen species, which promotes the degradation of AZO. In this paper, the possible intermediates of AZO were analyzed by LC-MS and DFT calculation. The degradation pathways of HA/ZVI/SPC and HA/ZVC/SPC were similar. In total, ten types of AZO intermediate products were detected in the HA/ZVI/SPC system, while nine types of products were detected in the HA/ZVC/SPC system. The main reactive functional groups of AZO were carbon–carbon double bonds, carboxyl groups and cyano groups, with the intermediate products generated by oxidative cracking and hydroxylation. The two HA/ZVM/SPC systems were able to maintain good stability and a high degradation capability after repeated cycles of use. The bioaccumulation and developmental toxicity factors of AZO decreased, according to the results of the toxicity evaluation. Overall, the heterogeneous Fenton system strengthened by HA was able to effectively remove AZO, showing significant promise for further optimization and practical application.

CRediT authorship contribution statement

Qiantong Liang: Writing – original draft, Validation, Software, Methodology, Investigation, Formal analysis, Data curation. **Chengyang Nan:** Writing – original draft, Validation, Software, Formal analysis. **Xiangwu Huang:** Writing – original draft, Validation, Formal analysis, Data curation. **Qingjin Lin:** Writing – original draft, Software, Formal analysis, Data curation. **Zhenyun Liang:** Writing – original draft, Data curation, Conceptualization. **Yu Huang:** Writing – original draft, Validation, Formal analysis, Data curation. **Peihong Zheng:** Writing – original draft, Data curation, Conceptualization. **Shoupeng Li:** Writing – review & editing, Resources, Project administration, Methodology, Funding acquisition, Conceptualization. **Shuiyu Sun:** Writing – review & editing, Resources, Project administration, Methodology, Funding acquisition, Conceptualization.

Declaration of competing interest

The authors declare that they have no known competing financial interests or personal relationships that could have appeared to influence the work reported in this paper.

Acknowledgments

The authors acknowledge the financial support of this study by the National Natural Science Foundation of China (No. 42277220) and Guangdong Provincial Youth Innovative Talent Project for Science and Technology (Natural Sciences) (Project No. 2023KQNCX198). We would like to thank Shiyanjia Lab (www.shiyanjia.com) for the support of SEM analysis. Furthermore, we also wish to thank the Analysis and Test Center, Guangdong University of Technology for offering the test.

Appendix A. Supplementary data

Supplementary data to this article can be found online at https://doi.org/10.1016/j.cej.2024.158126.

Data availability

No data was used for the research described in the article.

References

[1] M. Ikram, A. Haider, M. Imran, J. Haider, A. Ul-Hamid, A. Shahzadi, R. Malik, A. Kashaf Ul, W. Nabgan, G. Nazir, S. Ali, Graphitic-C(3)N(4)/chitosan-doped NiO nanostructure to treat the polluted water and their bactericidal with in silico molecular docking analysis, Int J Biol Macromol 227 (2023) 962–973, https://doi.org/10.1016/j.ijbiomac.2022.11.273.

[2] F. Cao, P. Wu, L. Huang, H. Li, L. Qian, S. Pang, L. Qiu, Short-term developmental effects and potential mechanisms of azoxystrobin in larval and adult zebrafish (Danio rerio), Aquat Toxicol 198 (2018) 129–140, https://doi.org/10.1016/j.aquatox.2018.02.023.

[3] A.A.A. Romeh, Phytoremediation of azoxystrobin and its degradation products in soil by P. major L. under cold and salinity stress, Pestic Biochem Physiol 142 (2017) 21–31, https://doi.org/10.1016/j.pestbp.2016.12.010.

[4] W.A. Battaglin, M.W. Sandstrom, K.M. Kuivila, D.W. Kolpin, M.T. Meyer, Occurrence of Azoxystrobin, Propiconazole, and Selected Other Fungicides in US Streams, 2005–2006, Water Air Soil Pollut. 218 (1–4) (2010) 307–322, https://doi.org/10.1007/s11270-010-0643-2.

[5] N. Berenzen, A. Lentzen-Godding, M. Probst, H. Schulz, R. Schulz, M. Liess, A comparison of predicted and measured levels of runoff-related pesticide concentrations in small lowland streams on a landscape level, Chemosphere 58 (5) (2005) 683–691, https://doi.org/10.1016/j.chemosphere.2004.05.009.

[6] J. Gao, X. Duan, K. O'Shea, D.D. Dionysiou, Degradation and transformation of bisphenol A in UV/Sodium percarbonate: Dual role of carbonate radical anion, Water Res 171 (2020) 115394, https://doi.org/10.1016/j.watres.2019.115394.

[7] X. Fu, X. Gu, S. Lu, M. Xu, Z. Miao, X. Zhang, Y. Zhang, Y. Xue, Z. Qiu, Q. Sui, Enhanced degradation of benzene in aqueous solution by sodium percarbonate activated with chelated-Fe(II), Chem. Eng. J. 285 (2016) 180–188, https://doi.org/10.1016/j.cej.2015.09.112.

[8] D. Wang, D. He, X. Liu, Q. Xu, Q. Yang, X. Li, Y. Liu, Q. Wang, B.J. Ni, H. Li, The underlying mechanism of calcium peroxide pretreatment enhancing methane production from anaerobic digestion of waste activated sludge, Water Res 164 (2019) 114934, https://doi.org/10.1016/j.watres.2019.114934.

[9] N.T. Hoa, H. Nguyen, L. Nguyen, K.N. Do, L.D. Vu, Efficient removal of ciprofloxacin in aqueous solutions by zero-valent metal-activated persulfate oxidation: A comparative study, J. Water Process Eng. 35 (2020) 101199, https://doi.org/10.1016/j.jwpe.2020.101199.

[10] X. Huang, Z. Yang, W. Dai, W. Song, Y. Gan, Z. Lian, W. Zhou, Z. Wu, L. Chen, X. Bai, Mediated biosynthesis of CdS QDs by EPS from Desulfovibrio desulfuricans sub sp. under carbon source-induced reinforcement, Journal of Hazardous Materials 459 (2023), https://doi.org/10.1016/j.jhazmat.2023.132146.

[11] M. Xing, W. Xu, C. Dong, Y. Bai, J. Zeng, Y. Zhou, J. Zhang, Y. Yin, Metal sulfides as excellent co-catalysts for H_2O_2 decomposition in advanced oxidation processes, Chem 4 (6) (2018) 1359–1372, https://doi.org/10.1016/j.chempr.2018.03.002.

[12] X. Li, C. Song, B. Sun, N. Yang, J. Gao, J. Zhu, Y. Liu, Model simulation and mechanism of Fe(0/II/III) cycle activated persulfate degradation of methylparaben based on hydroxylamine enhanced nano-zero-valent iron, J. Environ. Manage. 323 (2022) 116106, https://doi.org/10.1016/j.jenvman.2022.116106.

[13] W. Sang, Z. Li, M. Huang, X. Wu, D. Li, L. Mei, J. Cui, Enhanced transition metal oxide based peroxymonosulfate activation by hydroxylamine for the degradation of sulfamethoxazole, Chem. Eng. J. 383 (2020), https://doi.org/10.1016/j.cej.2019.123057.

[14] D. Han, J. Wan, Y. Ma, Y. Wang, M. Huang, Y. Chen, D. Li, Z. Guan, Y. Li, Enhanced decolorization of Orange G in a Fe(II)-EDDS activated persulfate process by accelerating the regeneration of ferrous iron with hydroxylamine, Chem. Eng. J. 256 (2014) 316–323, https://doi.org/10.1016/j.cej.2014.06.006.

[15] R. Yin, L. Hu, D. Xia, J. Yang, C. He, Y. Liao, Q. Zhang, J. He, Hydroxylamine promoted Fe(III)/Fe(II) cycle on ilmenite surface to enhance persulfate catalytic activation and aqueous pharmaceutical ibuprofen degradation, Catal. Today 358 (2020) 294–302, https://doi.org/10.1016/j.cattod.2019.04.081.

[16] T. Sun, Z.-Y. Jin, B. Deng, G. He, Q.-Y. Wang, M. Hu, Z. Han, Z. Zheng, J. Zhao, J. Yun, J. Zhao, Y. Zhu, Z. Pan, X. Li, Z.-T. Hu, Visible-light-driven photo-Fenton oxidation enhanced by Fe/Bi-nanocrystal phase transformation as a universal way for various organic pollutants mineralization, Chem. Eng. J. 481 (2024), https://doi.org/10.1016/j.cej.2024.148732.

[17] S. Ma, Y. Gan, W. Song, W. Dai, Z. Yang, R. Yang, X. Huang, J. Li, Z. Wu, L. Chen, Radical-/non-radical-mediated catalyst activation of peroxymonosulfate for efficient atrazine degradation, Chemosphere 320 (2023) 138034, https://doi.org/10.1016/j.chemosphere.2023.138034.

[18] X. Huang, W. Song, Z. Yang, Z. Wu, L. Chen, Q. Liang, J. Li, C. Tu, G. Zheng, W. Zhou, X. Zhang, The important role of EPS in mediated biosynthesis of CdS QDs: Comparative study of EPS-intact and EPS-free, J. Hazard. Mater. 474 (2024), https://doi.org/10.1016/j.jhazmat.2024.134760.

[19] S. Correa-Sanchez, G.A. Peñuela, Peracetic acid-based advanced oxidation processes for the degradation of emerging pollutants: A critical review, J. Water Process Eng. 49 (2022) 102986, https://doi.org/10.1016/j.jwpe.2022.102986.

[20] Y. Ren, M. Shi, W. Zhang, D.D. Dionysiou, J. Lu, C. Shan, Y. Zhang, L. Lv, B. Pan, Enhancing the Fenton-like Catalytic Activity of nFe(2)O(3) by MIL-53(Cu) Support: A Mechanistic Investigation, Environ Sci Technol 54 (8) (2020) 5258–5267, https://doi.org/10.1021/acs.est.0c00203.

[21] X. Huang, T. Zhu, W. Duan, S. Liang, G. Li, W. Xiao, Comparative studies on catalytic mechanisms for natural chalcopyrite-induced Fenton oxidation: Effect of chalcopyrite type, J. Hazard. Mater. 381 (2020) 120998, https://doi.org/10.1016/j.jhazmat.2019.120998.

[22] F.A. Ghori, Y. Wu, X. Lin, Y. He, Q. Yu, H. Chen, G. Xue, Insight into simultaneous urea hydrolysis and total nitrogen removal in textile printing wastewater: Focus on the impact of sodium sulfate salinity, J. Environ. Manage. 370 (2024) 122551, https://doi.org/10.1016/j.jenvman.2024.122551.

[23] P. Zhang, S. Yuan, P. Liao, Mechanisms of hydroxyl radical production from abiotic oxidation of pyrite under acidic conditions, Geochim. Cosmochim. Acta 172 (2016) 444–457, https://doi.org/10.1016/j.gca.2015.10.015.

[24] T. Lu, Q. Chen, Realization of conceptual density functional theory and information-theoretic approach in multiwfn program, Conceptual Density Functional Theory (2022) 631–647, https://doi.org/10.1002/9783527829941.ch31.

[25] J. Duan, S.Y. Pang, Z. Wang, Y. Zhou, Y. Gao, J. Li, Q. Guo, J. Jiang, Hydroxylamine driven advanced oxidation processes for water treatment: A review, Chemosphere 262 (2021) 128390, https://doi.org/10.1016/j.chemosphere.2020.128390.
[26] P. Avetta, A. Pensato, M. Minella, M. Malandrino, V. Maurino, C. Minero, K. Hanna, D. Vione, Activation of persulfate by irradiated magnetite: implications for the degradation of phenol under heterogeneous photo-Fenton-like conditions, Environ Sci Technol 49 (2) (2015) 1043–1050, https://doi.org/10.1021/es503741d.
[27] Y. Jin, S.-P. Sun, X. Yang, X.D. Chen, Degradation of ibuprofen in water by FeII-NTA complex-activated persulfate with hydroxylamine at neutral pH, Chem. Eng. J. 337 (2018) 152–160, https://doi.org/10.1016/j.cej.2017.12.094.
[28] Y.-T. Lin, C. Liang, C.-W. Yu, Trichloroethylene degradation by various forms of iron activated persulfate oxidation with or without the assistance of ascorbic acid, Ind. Eng. Chem. Res. 55 (8) (2016) 2302–2308, https://doi.org/10.1021/acs.iecr.5b04352.
[29] H. Zeng, S. Liu, B. Chai, D. Cao, Y. Wang, X. Zhao, Enhanced photoelectrocatalytic decomplexation of Cu-EDTA and Cu recovery by persulfate activated by UV and cathodic reduction, Environ Sci Technol 50 (12) (2016) 6459–6466, https://doi.org/10.1021/acs.est.6b00632.
[30] Y. Li, H. Dong, L. Li, J. Xiao, S. Xiao, Z. Jin, Efficient degradation of sulfamethazine via activation of percarbonate by chalcopyrite, Water Res 202 (2021) 117451, https://doi.org/10.1016/j.watres.2021.117451.
[31] Z. Mo, Z. Tan, J. Liang, Z. Guan, X. Liao, J. Jian, H. Liu, Y. Li, W. Dai, S. Sun, Iron-rich sludge biochar triggers sodium percarbonate activation for robust sulfamethoxazole removal: Collaborative roles of reactive oxygen species and electron transfer, Chem. Eng. J. 457 (2023), https://doi.org/10.1016/j.cej.2022.141150.
[32] M. Danish, X. Gu, S. Lu, A. Ahmad, M. Naqvi, U. Farooq, X. Zhang, X. Fu, Z. Miao, Y. Xue, Efficient transformation of trichloroethylene activated through sodium percarbonate using heterogeneous zeolite supported nano zero valent iron-copper bimetallic composite, Chem. Eng. J. 308 (2017) 396–407, https://doi.org/10.1016/j.cej.2016.09.051.
[33] W. Xiang, T. Zhou, Y. Wang, M. Huang, X. Wu, J. Mao, X. Lu, B. Zhang, Catalytic oxidation of diclofenac by hydroxylamine-enhanced Cu nanoparticles and the efficient neutral heterogeneous-homogeneous reactive copper cycle, Water Res 153 (2019) 274–283, https://doi.org/10.1016/j.watres.2019.01.024.
[34] J. Tang, J. Wang, MOF-derived three-dimensional flower-like FeCu@C composite as an efficient Fenton-like catalyst for sulfamethazine degradation, Chem. Eng. J. 375 (2019), https://doi.org/10.1016/j.cej.2019.122007.
[35] S. Sajjadi, A. Khataee, R.D.C. Soltani, N. Bagheri, A. Karimi, A.E.F. Azar, Implementation of magnetic Fe3O4@ZIF-8 nanocomposite to activate sodium percarbonate for highly effective degradation of organic compound in aqueous solution, J. Ind. Eng. Chem. 68 (2018) 406–415, https://doi.org/10.1016/j.jiec.2018.08.016.
[36] H. Luo, Y. Zeng, Y. Cheng, D. He, X. Pan, Activation of peroxymonosulfate by iron oxychloride with hydroxylamine for ciprofloxacin degradation and bacterial disinfection, Sci Total Environ 799 (2021) 149506, https://doi.org/10.1016/j.scitotenv.2021.149506.
[37] X. Chen, W.-X. Zhang, Z.-L. Chen, X.-W. Yao, M.-L. Chen, L.-Y. Tong, W. Qian, P.-R. Guo, L.-J. Kong, Z.-H. Diao, Efficient activation of persulfate by metallic sulfide mineral for the efficient removal of pesticides: Performance, radical generation and mechanism, J. Clean. Prod. 421 (2023), https://doi.org/10.1016/j.jclepro.2023.138521.
[38] C.M. Hung, C.W. Chen, C.P. Huang, M.L. Tsai, C.H. Wu, Y.L. Lin, Y.R. Cheng, C. D. Dong, Efficacy and cytotoxicity of engineered ferromanganese-bearing sludge-derived biochar for percarbonate-induced phthalate ester degradation, J Hazard Mater 422 (2022) 126922, https://doi.org/10.1016/j.jhazmat.2021.126922.
[39] C.M. Hung, C.P. Huang, C.W. Chen, C.H. Wu, Y.L. Lin, C.D. Dong, Activation of percarbonate by water treatment sludge-derived biochar for the remediation of PAH-contaminated sediments, Environ Pollut 265 (Pt B) (2020) 114914, https://doi.org/10.1016/j.envpol.2020.114914.
[40] J. Liang, S. Zhang, M. Ye, J. Huang, X. Yang, S. Li, S. Huang, S. Sun, Improving sewage sludge dewaterability with rapid and cost-effective in-situ generation of Fe2+ combined with oxidants, Chem. Eng. J. 380 (2020), https://doi.org/10.1016/j.cej.2019.122499.
[41] X. Zhou, Q. Wang, G. Jiang, X. Zhang, Z. Yuan, Improving dewaterability of waste activated sludge by combined conditioning with zero-valent iron and hydrogen peroxide, Bioresour Technol 174 (2014) 103–107, https://doi.org/10.1016/j.biortech.2014.10.009.
[42] H. Xu, D. Wang, J. Ma, T. Zhang, X. Lu, Z. Chen, A superior active and stable spinel sulfide for catalytic peroxymonosulfate oxidation of bisphenol S, Appl Catal B 238 (2018) 557–567, https://doi.org/10.1016/j.apcatb.2018.07.058.
[43] Z. Zhou, G. Ye, Y. Zong, Z. Zhao, D. Wu, Improvement of Fe(III)/percarbonate system by molybdenum powder and tripolyphosphate: Co-catalytic performance, low oxidant consumption, pH-dependent mechanism, J Hazard Mater 464 (2024) 132924, https://doi.org/10.1016/j.jhazmat.2023.132924.
[44] S. Zhu, X. Li, J. Kang, X. Duan, S. Wang, Persulfate activation on crystallographic manganese oxides: mechanism of singlet oxygen evolution for nonradical selective degradation of aqueous contaminants, Environ Sci Technol 53 (1) (2019) 307–315, https://doi.org/10.1021/acs.est.8b04669.
[45] X. Liu, S. He, Y. Yang, B. Yao, Y. Tang, L. Luo, D. Zhi, Z. Wan, L. Wang, Y. Zhou, A review on percarbonate-based advanced oxidation processes for remediation of organic compounds in water, Environ Res 200 (2021) 111371, https://doi.org/10.1016/j.envres.2021.111371.
[46] J. Xiao, Y. Li, H. Dong, Z. Pang, M. Zhao, D. Huang, J. Dong, L. Li, Highly efficient activation of peracetic acid via zero-valent iron-copper bimetallic nanoparticles (nZVIC) for the oxidation of sulfamethazine in aqueous solution under neutral condition, Appl Catal B 340 (2024), https://doi.org/10.1016/j.apcatb.2023.123183.
[47] K. Liu, J.C. Yu, H. Dong, J.C.S. Wu, M.R. Hoffmann, Degradation and mineralization of carbamazepine using an electro-fenton reaction catalyzed by magnetite nanoparticles fixed on an electrocatalytic carbon fiber textile cathode, Environ. Sci. Technol. 52 (21) (2018) 12667–12674, https://doi.org/10.1021/acs.est.8b03916.
[48] Y. Nie, C. Hu, J. Qu, L. Zhou, X. Hu, Photoassisted degradation of azodyes over FeOxH2x-3/Fe0 in the presence of H2O2 at neutral pH values, Environ. Sci. Tech. 41 (13) (2007) 4715–4719, https://doi.org/10.1021/es062513x.
[49] M. Devaraj, R. Saravanan, R. Deivasigamani, V.K. Gupta, F. Gracia, S. Jayadevan, Fabrication of novel shape Cu and Cu/Cu2O nanoparticles modified electrode for the determination of dopamine and paracetamol, J. Mol. Liq. 221 (2016) 930–941, https://doi.org/10.1016/j.molliq.2016.06.028.
[50] Y. Zhang, J. Fan, B. Yang, W. Huang, L. Ma, Copper-catalyzed activation of molecular oxygen for oxidative destruction of acetaminophen: The mechanism and superoxide-mediated cycling of copper species, Chemosphere 166 (2017) 89–95, https://doi.org/10.1016/j.chemosphere.2016.09.066.
[51] K.L. Deutsch, B.H. Shanks, Active species of copper chromite catalyst in C–O hydrogenolysis of 5-methylfurfuryl alcohol, J. Catal. 285 (1) (2012) 235–241, https://doi.org/10.1016/j.jcat.2011.09.030.
[52] Y. Zhang, Z. Guan, X. Liao, Y. Huang, Z. Huang, Z. Mo, B. Yin, X. Zhou, W. Dai, J. Liang, S. Sun, Defluorination of perfluorooctanoic acid and perfluorooctane sulfonic acid by heterogeneous catalytic system of Fe-Al(2)O(3)/O(3): Synergistic oxidation effects and defluorination mechanism, Sci. Total Environ. 915 (2024) 169675, https://doi.org/10.1016/j.scitotenv.2023.169675.
[53] L. Guo, F. Chen, X. Fan, W. Cai, J. Zhang, S-doped α-Fe2O3 as a highly active heterogeneous Fenton-like catalyst towards the degradation of acid orange 7 and phenol, Appl Catal B 96 (1–2) (2010) 162–168, https://doi.org/10.1016/j.apcatb.2010.02.015.
[54] D. Wilson, M.A. Langell, XPS analysis of oleylamine/oleic acid capped Fe_3O_4 nanoparticles as a function of temperature, Appl. Surf. Sci. 303 (2014) 6–13, https://doi.org/10.1016/j.apsusc.2014.02.006.
[55] Z. Yang, Y. Liu, J. Wang, MOF-derived Cu0/C activation of molecular oxygen for efficient degradation of sulfamethazine, Chem. Eng. J. 427 (2022), https://doi.org/10.1016/j.cej.2021.131961.
[56] X. Fan, Q. Lin, K. Xu, J. Zheng, J. Sun, H. Fu, Y. Liu, Y. Ma, J. He, Activation of peroxydisulfate degradation of ciprofloxacin by nitrogen-doped modified graphitized iron-based carbon materials: The transition from free to nonfree radicals, Sep. Purif. Technol. 316 (2023), https://doi.org/10.1016/j.seppur.2023.123783.
[57] L. Qin, H. Ye, C. Lai, S. Liu, X. Zhou, F. Qin, D. Ma, B. Long, Y. Sun, L. Tang, M. Yan, W. Chen, W. Chen, L. Xiang, Citrate-regulated synthesis of hydrotalcite-like compounds as peroxymonosulfate activator - Investigation of oxygen vacancies and degradation pathways by combining DFT, Appl Catal B 317 (2022), https://doi.org/10.1016/j.apcatb.2022.121704.